SPACE AND ENERGY DEPENDENT NEUTRON SLOWING DOWN TIME IN GRAPHITE by FRANCIS W GIBBONS

Course XXII Sept 1967

SPACE AND ENERGY DEPENDENT NEUTRON SLOWING DOWN TIME IN GRAPHITE

by

Francis W. Gibbons
Ensign, United States Navy

B.S., United States Naval Academy
(1966)

SUBMITTED IN PARTIAL FULFILLMENT OF THE
REQUIREMENTS FOR THE DEGREE OF
MASTER OF SCIENCE

at the

MASSACHUSETTS INSTITUTE OF TECHNOLOGY

September, 1967

Signature of Author. . . . . .

Department of Nuclear Engineering
September, 1967

Certified by. . . . . .

Thesis Supervisor

ABSTRACT

SPACE AND ENERGY DEPENDENT NEUTRON SLOWING DOWN TIME IN GRAPHITE

Submitted to the Department of Nuclear Engineering on September 26, 1967 in partial fulfillment of the requirements for the degree of Master of Science.

A 4 foot cube, graphite moderating assembly was constructed at the M.I.T. Rockefeller Van de Graaff accelerator. Using the pulsed neutron experimental installation, a neutron burst of 200 nsec width was injected into the center of the assembly. Prompt gamma radiation from a neutron resonance capture by an indicator foil in the moderator was measured, with a 3 inch x 3 inch sodium iodide scintillation detector, as a function of time after the neutron pulse. The energy dependence of slowing down time was experimentally measured by using resonance absorber foils of cadmium, indium, and gold with isolated resonances of 0.2, 1.46 and 5.0 eV respectively. By varying the distance of the foil from the source, the spatial dependence of slowing down time was also investigated. Comparisons are made with slowing down theory. The experimental results, together with their estimated uncertainties, are tabulated below:

	t_m (μsec)		
r(cm)	0.2	1.46	5.0
12.5	47.50 ± 3.00	19.75 ± .50	11.25 ± .25
18.0	47.25 ± 2.25	19.37 ± .25	10.10 ± .25
28.0	47.25 ± 2.25	19.00 ± .50	10.87 ± .25
37.5	-	20.00 ± .50	11.13 ± .37
44.0	-	-	12.50 ± .25
44.5	49.75 ± 2.25	21.62 ± .50	-

Thesis Supervisor: Franklyn M. Clikeman

Title: Assistant Professor of Nuclear Engineering

TABLE OF CONTENTS

TABLE OF CONTENTS (Continued)

CHAPTER 1

Introduction

In his M.I.T. Ph.D. thesis, Adamantiades (1) demonstrated that the pulsed neutron technique using a resonance absorber as a point indicator could be used to measure system transient effects such as the slowing down time. He designed and installed an experimental installation for pulsed neutron experiments, and made some measurements in water. Vaughan (2) refined Adamantaides' system, and measured the spatial dependence of slowing down time in water for three different resonance absorbers. Möller has carried out extensive experiments in the field of neutron slowing down for both light (3,4) and heavy (5) water. However, there does not appear to be any published measurements of the slowing down time for heavier moderators. Therefore, in this present experiment, the pulsed technique has been expanded to investigate slowing down time in graphite.

In the pulsed neutron method, a short monoenergetic burst of neutrons is injected into the moderating medium at a point. The neutrons, originally high energy, gradually slow down by elastic collisions with the moderating medium. If a neutron indicator is incorporated into the moderating medium, it is possible to measure the time difference between pulse injection and neutron arrival at the indicator. A

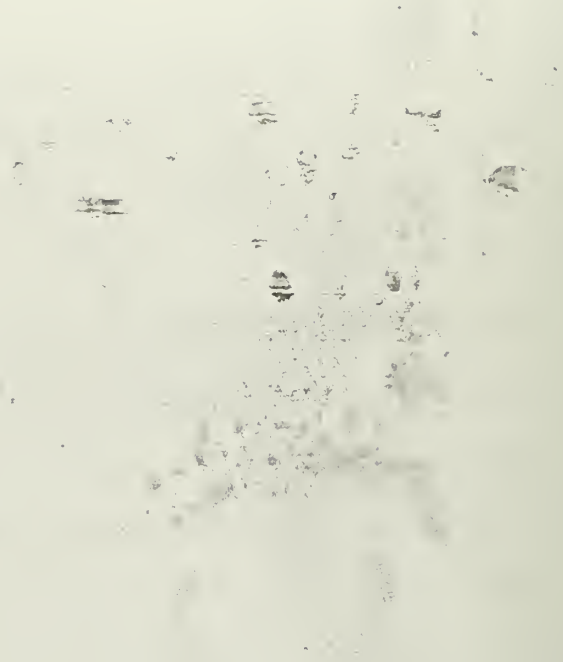

time distribution is formed from many time differences, measured under the exact same conditions.

Since most materials emit prompt gamma rays upon the capture of a neutron, detection of these gamma rays provides one method by which the time behavior of neutron captures may be followed after the pulse. If an absorber with a strong, isolated neutron capture resonance is incorporated into the moderating system as a point indicator, then the reaction rate of the neutron flux with the absorption resonance is proportional to the time dependent flux at that point, for neutrons with energies equal to the resonance energy. That is, the neutron density (or flux) $N(r,E_r,t)$

N - neutron density

r - distance from source

E_r - energy of absorber resonance

t - time

can be measured. Thus, variation of the position of the absorber and the use of different resonance absorbers should yield the time, space, and energy variation of the neutron density following the pulsing of the assembly.

By using the M.I.T. Rockefeller Van de Graaff accelerator as a source of high energy protons, high energy neutrons were obtained by the $Li^7(p,n)Be^7$ nuclear reaction. The lithium target was located at the center of a large assembly of graphite, thus approximating a point source in an infinite medium. The accelerator beam was pulsed by an external

pulsing system after the protons had been accelerated. The pulse width used in these experiments was 200 nsec. Enough time was allowed to elapse between pulses so that all transient neutron effects from one pulse would die out before the next pulse was injected. Absorber foils of cadmium, indium, and gold, with isolated resonances located at 0.2 eV, 1.46 eV, and 5.0 eV respectively, were used to sample the neutron flux at these energies. A detecting and analyzing system was assembled that was capable of indicating the time difference between pulse injection and the resonance capture of a neutron. The most probable time difference from injection to resonance capture was assumed to be the neutron slowing down time for that energy at that position.

The material in this thesis is organized as follows: Chapter 2 is concerned with slowing down theory; the experimental facilities are described in Chapter 3; the performance of the experiments is described in Chapter 4; and the results are presented and discussed.

References for Chapter 1

1. A.G. Adamantiades, Ph.D. Thesis, Department of Nuclear Engineering M.I.T., (1966).

2. J.E. Vaughan, M.S. Thesis, Department of Nuclear Engineering M.I.T., (1967).

3. E. Möller and Sjostrand, N.G., Report RFX-248, Chalmers University of Technology, Sweden (1963); Proc. Ins. Conf. Neutron Thermalization, BNL-719, pp. 966 - 976.

4. E. Möller, Measurement of the Neutron Slowing-Down Time Distribution at 1.46 eV and Its Space Dependence in Water, Arkiv for Fysik, 31, 255 (1965).

5. E. Möller, Report AE-216, Aktiebotaget Atomenergi, Sweden (1962).

CHAPTER 2

Theory

2.1 General

The analytical treatment of pulsed neutron assemblies requires a mathematical solution of the general transport equation. If an expression representing the neutron density as a function of time, energy, and space, and satisfying the Boltzmann transport equation with its source and boundary conditions can be found, the behavior of neutrons in the system can be completely described.

Unfortunately, no exact solution of the Boltzmann equation, in all its generality, has ever been found; but approximate solutions are available. Of these solutions, only a few may be verified because not all quantities can be measured experimentally.

The quantity most readily measured experimentally in the slowing down region is the neutron slowing down time (t_m). This is the time at which the neutron density at some energy (E) is maximum and can be found by setting the derivative of N(r,E,t)

N - neutron density

r - distance from source

E - neutron energy

t - time

with respect to time equal to zero.

It is also possible to measure the mean slowing down time (<t>) which is also defined at the first time moment. The time moments are integral quantities defined as:

$$\langle t^n(r,v)\rangle = \int_0^\infty t^n\, N(v,t)\, dt \Big/ \int_0^\infty N(v,t)\, dt \qquad (2.1.1)$$

N(v,t) - neutron density as a function of space and energy (velocity)

t - time

Both the time to maximum or the slowing down time, and mean slowing down time may be measured experimentally as a function of space and neutron energy.

In this experiment, the source may be considered isotropic and a delta function in time, energy, and space. Although the neutron source energy does vary with the angle in the laboratory system, this source term can be neglected because it appears in the denominator of the expressions for the time distributions, and it is much greater than the energy at which the time distribution is measured. For example, one expression for the neutron slowing down flux in hydrogen is:

$$\varphi(v,t) = S\cdot(vt/\gamma_s)^2 \cdot\exp(-vt/\gamma_s)\cdot(1-v/v_o+2\gamma_s/v_o t)+ 2S\cdot v_o/v\cdot\delta(v-v_o)\cdot\exp(-v_o t/\gamma_s) \qquad (2.1.2)$$

φ - neutron flux

v - neutron velocity

S - source strength

γ_s - scattering mean free path

v_o - neutron source velocity

t - time

However, because $v_o >> v$, equation (2.1.2) simplifies to:

$$\varphi(v,t) = S \cdot (vt/\gamma_s)^2 \cdot \exp(-vt/\gamma_s) \qquad (2.1.3)$$

Except for positions closer than three mean free paths away from the physical boundary of the assembly, the spatial boundary conditions are those of an infinite medium. For positions closer than three mean paths, leakage must be taken into account.

In the energy region lying above a few tenths of an eV, the nuclei of the moderating assembly can be considered free and at rest. For lower energies, however, the molecular structure of the moderator becomes important.

Any absorption which occurs in the moderating assembly will effect the time distribution. Those neutrons which take longer to slow down, i.e. have more collisions, to energy (v) will have a greater probability of being absorbed. Thus, absorption contributes to a decrease in t_m. In graphite, the absorption cross section is very small; and absorption effects may be neglected.

2.2 Space Independent Slowing Down Theory

If, in addition to an infinite medium, we assume a uniformly distributed source instead of a spatial delta function source, the spatial dependence is removed from the

Boltzmann Equation. The equation reduces to:

$$1/v \cdot \delta\varphi(v,t)/\delta t = -[\varepsilon_s(v)+\varepsilon_a(v)]\varphi(v,t)+ \int \varphi(v',t)\cdot\varepsilon(v'\longrightarrow v)\, dv' + S\cdot\delta(v-v_o)\cdot\delta(t) \qquad (2.2.1)$$

$\varphi(v,t)$ - neutron flux as a function of space and energy (velocity)

ε_s - macroscopic scattering cross section

ε_a - macroscopic absorption cross section

ε - removal cross section

s - source strength (n/cm^2-sec)

v_o - source energy

$\delta(\ )$ - Dirac delta function

Unfortunately, for a heavier than water moderator, it is very difficult to obtain an expression for the flux, and hence, for the slowing down time. Using a method introduced by Marshak (1) the time moments can be obtained exactly. A few of the moments, in terms of the moderator mass number, obtained by Adamantiades (2) are given in Table I, of his thesis. Once the time moments have been determined, trial functions can be found to fit these moments.

Marshak and vonDardel (3) suggest using the function:

$$\varphi(x) = A\cdot x^{-1+2/(1-r^2)}\cdot\exp(-x-b/x) \qquad (2.2.2)$$

A - normalization constant

$x = vt/\gamma_s$ where γ_s - scattering mean free path

$r = (M-m)/(M+m)$

M - mass of moderator

m - mass of neutron

b - a parameter

which gives the right asymptotic dependence for the higher positive moments. vonDardel varies the parameter (b) with (r) while Marshak treats it as a constant.

For heavier elements, the time dependent neutron density distribution approaches a narrow Gaussian in shape. Thus, for heavier elements, t_m should approximately equal $\langle t \rangle$.

Adamantiades gives a complete discussion of the time moment method in Chapter II of his thesis. He also mentions other methods, and gives a number of references dealing with the problem of a heavier than water moderator. None of these references, however, specifically give results for graphite assemblies.

2.3 Space Dependent Slowing Down Theory

When the neutron source is localized, as in this experiment, the effects of diffusion during moderation must be taken into account. The problem becomes much more complicated since the transport equation is now a function of three, rather than two variables.

As in the space independent case, Adamantiades in Chapter II of his thesis discusses the theoretical work which has been done in this area. This concludes a solution by Dyad'kin and Batalina (4), for the space-energy-time neutron density distribution assuming no absorption, constant

scattering cross section, and isotropic scattering. The expression involves three factors which are complicated; and require coefficients which are dependent on the medium being examined. The authors also give a simplified expression for t_m, which is:

$$t_{max} = 2\gamma_s/v\pi\cdot(2-\beta\mu/\sqrt{r^2+\beta^2\mu^2})\cdot [1-2\alpha/3\cdot(1-\beta\mu/\sqrt{r^2+\beta^2\mu^2})]^{-1} \qquad (2.3.1)$$

γ_s - scattering mean free path

v - neutron velocity

π - average logarithmic energy decrement

μ - neutron lethargy

α - parameter which depends on the moderating medium

β - parameter which depends on the moderating medium

r - distance from source

Results are given for sand and water mixtures.

Claesson (5) has also determined the space dependent neutron density distribution for both a point and plane source assuming zero absorption, isotropic scattering, and constant mean free path. Although his method can be extended to moderators of arbitrary mass, curves are only given for the case of water at the indium resonance. These curves show however, that past 10 cm the slowing down time is strongly dependent on neutron energy at birth.

Adamantiades also develops a method of calculating time moments using an iterative solution of the stationary transport equation. The nth time moment is expressed

as:

$$\langle t^n \rangle = \varphi^{(n)}/\varphi^{(o)} \qquad (2.3.2)$$

$$H\varphi^{(o)} = -S(r,v,\mu) \qquad (2.3.3)$$

$$H\varphi^{(n)} + n/v \cdot \varphi^{(n-1)} = 0 \qquad (2.3.4)$$

$$H = [-\mu \cdot \nabla - \varepsilon_t + \int dv' \int d\mu' \; \varepsilon_s(v' \longrightarrow v, \mu' \longrightarrow \mu)] \qquad (2.3.5)$$

r,v,μ - vectors for position, velocity and solid angle, respectively

ε_t - total macroscopic absorption cross section.

Any calculational method suitable to solve the steady state can be used to solve for the flux moments.

David Diamond, a graduate student at M.I.T., has kindly supplied theoretical time distributions at the gold and indium resonances for a number of spatial points, using the diffusion approximation. A distribution for each foil at a distance from the source of 18 cm is shown in Figure 2.1 (a) and (b).

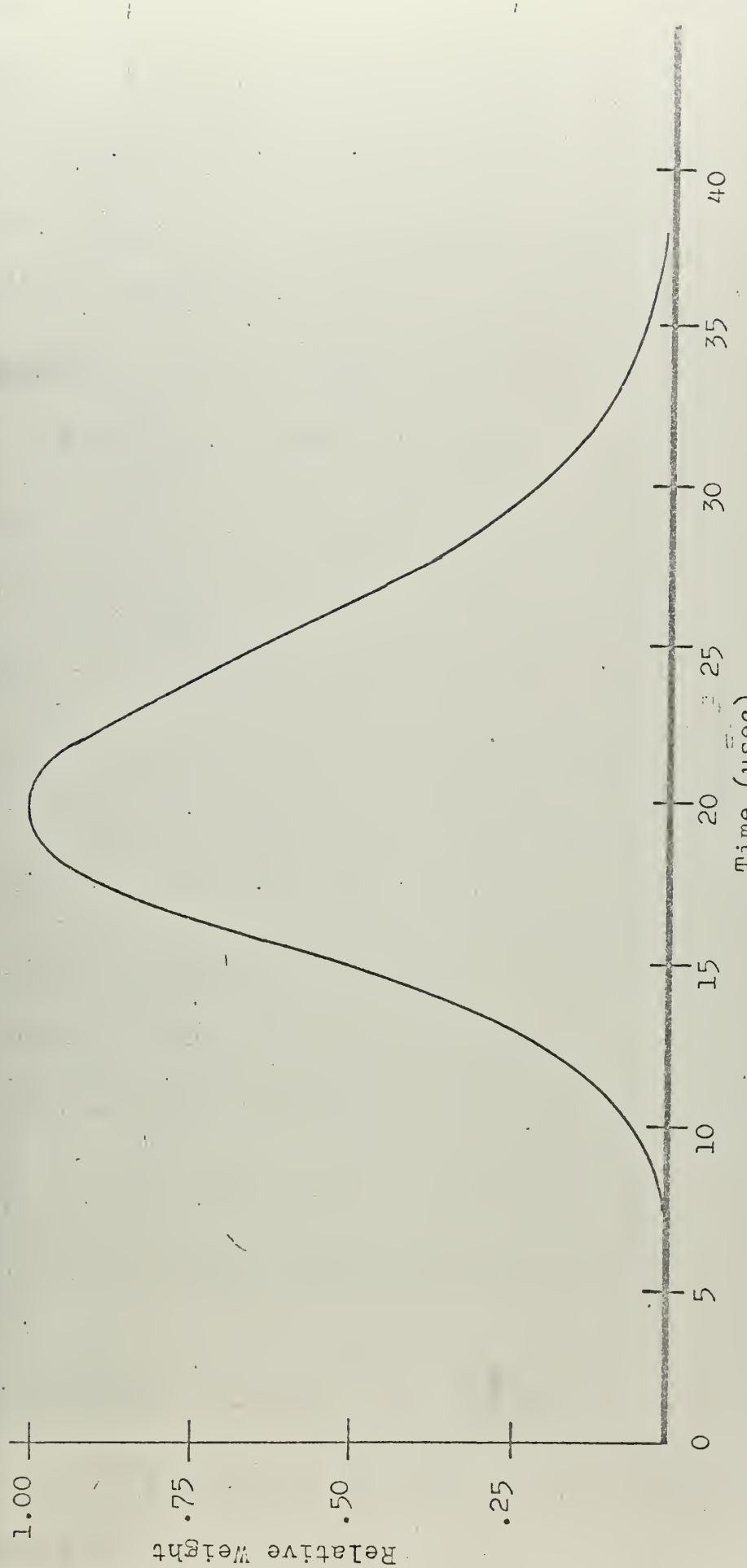

Figure 2.1 (a) Theoretical Time Distribution at 1.46 eV and 18 cm Away From the Source

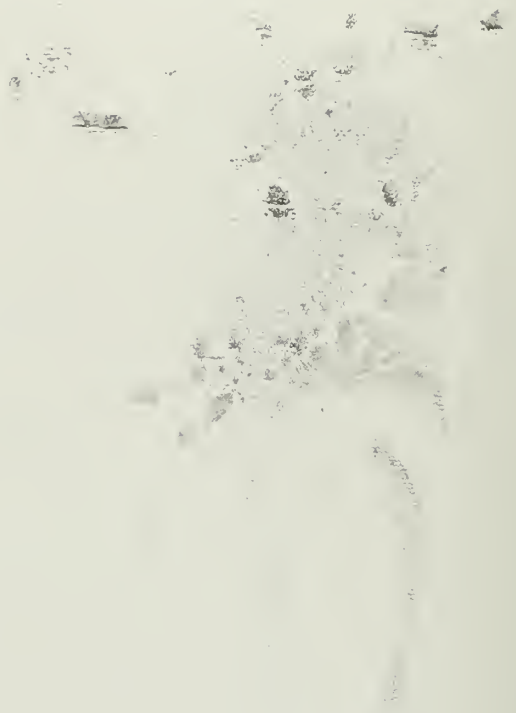

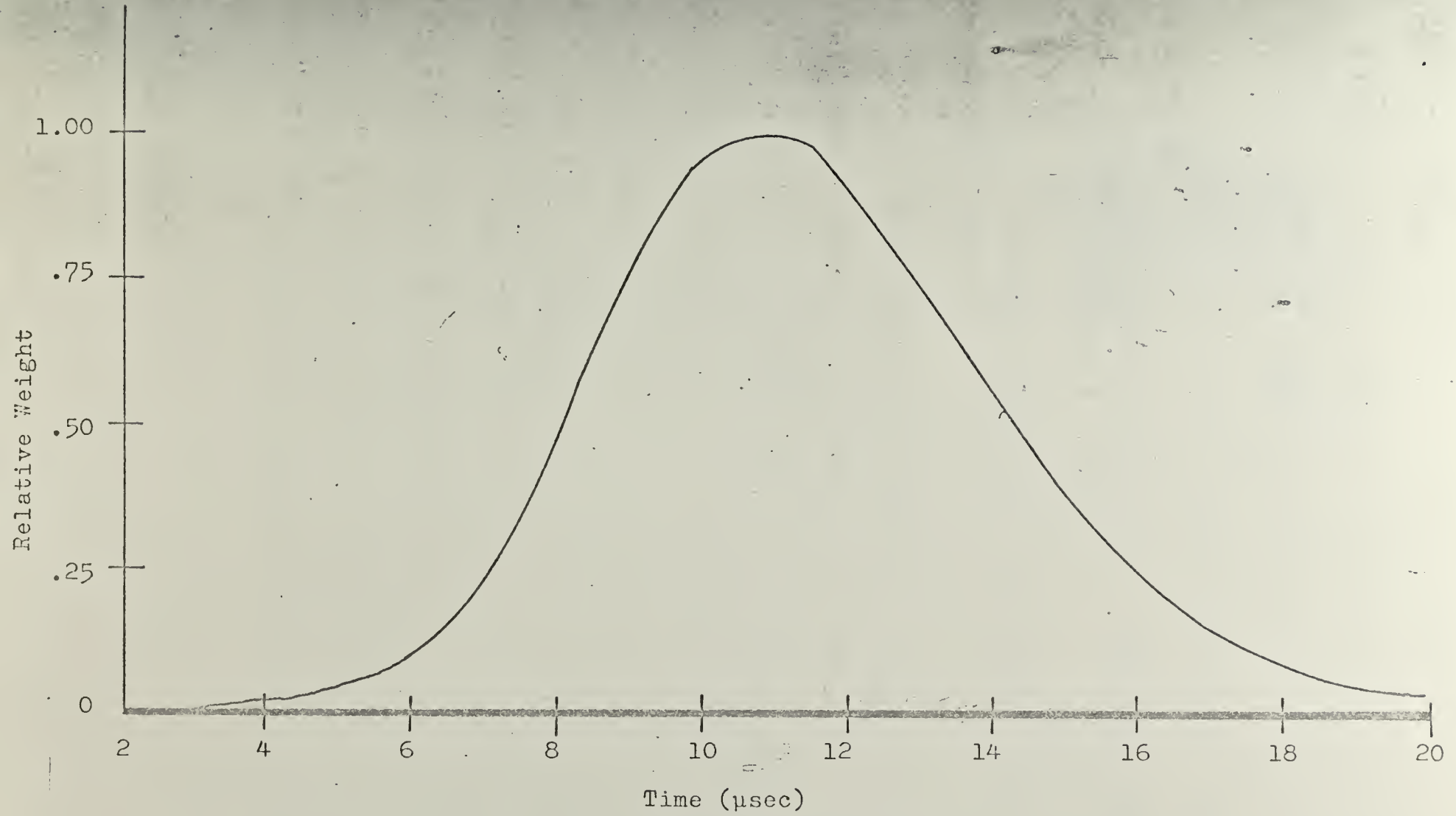

Figure 2.1 (b) Theoretical Time Distribution at 5.0 eV and 18 cm Away From the Source

References for Chapter 2

1. R.E. Marshak, Review of Modern Physics, 19, 185 (1947).

2. A.G. Adamantiades, Ph.D. Thesis, Department of Nuclear Engineering, M.I.T., (1966).

3. G.F. vonDardel, Trans, Roy. Inst. Techn., Stockholm, 75 (1954).

4. I.G. Dyad'kin and E.P. Batalina, Atomnaya Energiya 10, No. 1,5 (1961); Reactor Sci. Techn. 16, 103 (1962).

5. A. Claesson, Report AE-71, Aktiebotaget Atomenergi, Sweden (1962).

CHAPTER 3

Experimental Equipment

3.1 General Description

The equipment necessary for measuring neutron transient effects by the pulsed source method can be grouped into six categories:

1) The neutron source.
2) A method for pulsing the source.
3) The moderating assembly.
4) A system for detecting, analyzing and storing data.
5) A system to monitor the experimental equipment.
6) A normalizing system to insure consistent data.

The general layout of the experimental system showing the major components is given in Figure 3.1.

The neutron source consisted of a target of natural lithium, located approximately in the center of the moderating assembly, bombarded by 2.4 MeV protons to produce the $Li^7(p,n)Be^7$ reaction. The high energy protons were produced by a Van de Graaff electrostatic accelerator. The pulsing system electrostatically deflected the proton beam off the lithium target, allowing it to strike the target for a short time.

Thus, the pulse of fast neutrons produced at the target was ejected into the center of the moderating assembly.

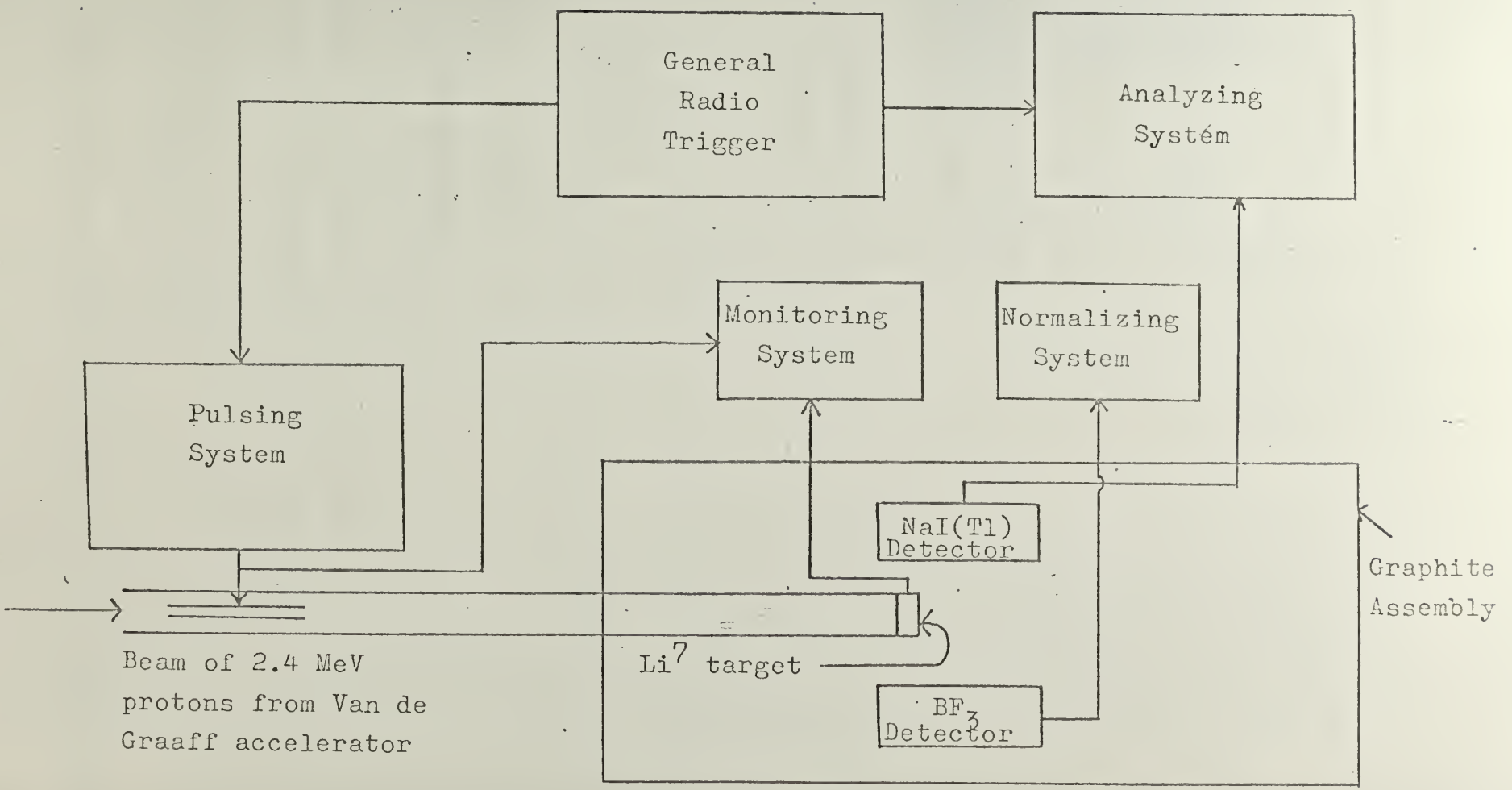

Figure 3.1 Block Diagram of Major Systems

These neutrons were then slowed down by elastic collisions in the medium, and their time distribution was measured by the detecting and analyzing system. This system consisted of the conventional detector-preamplifier-amplifier array, plus electronic equipment for pulse height discrimination and time analysis combined with a multi-channel analyzer to store the data. There was a common link between the pulsing and the analyzing system which provided a zero time reference.

The monitoring system was used to control the performance of the pulsing system, and thus to optimize the quality of the neutron pulse. The normalizing system yielded the time integrated neutron flux for each experiment performed. This information was necessary to properly carry out background subtraction.

A more detailed description of the experimental equipment will be given in the sections to follow.

3.2 The Mechanical Layout

A plan view of the mechanical layout of the system is given in Figure 3.2. Only a brief description of the system will be given here since a thorough, detailed description of the system will be given by Adamantiades (1), who actually constructed the system.

Since the experimental apparatus was positioned on the floor below the accelerator, the protons were accelerated

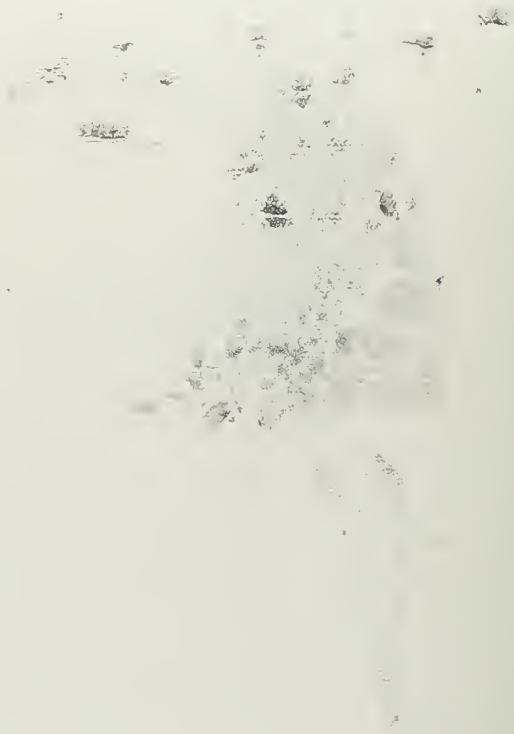

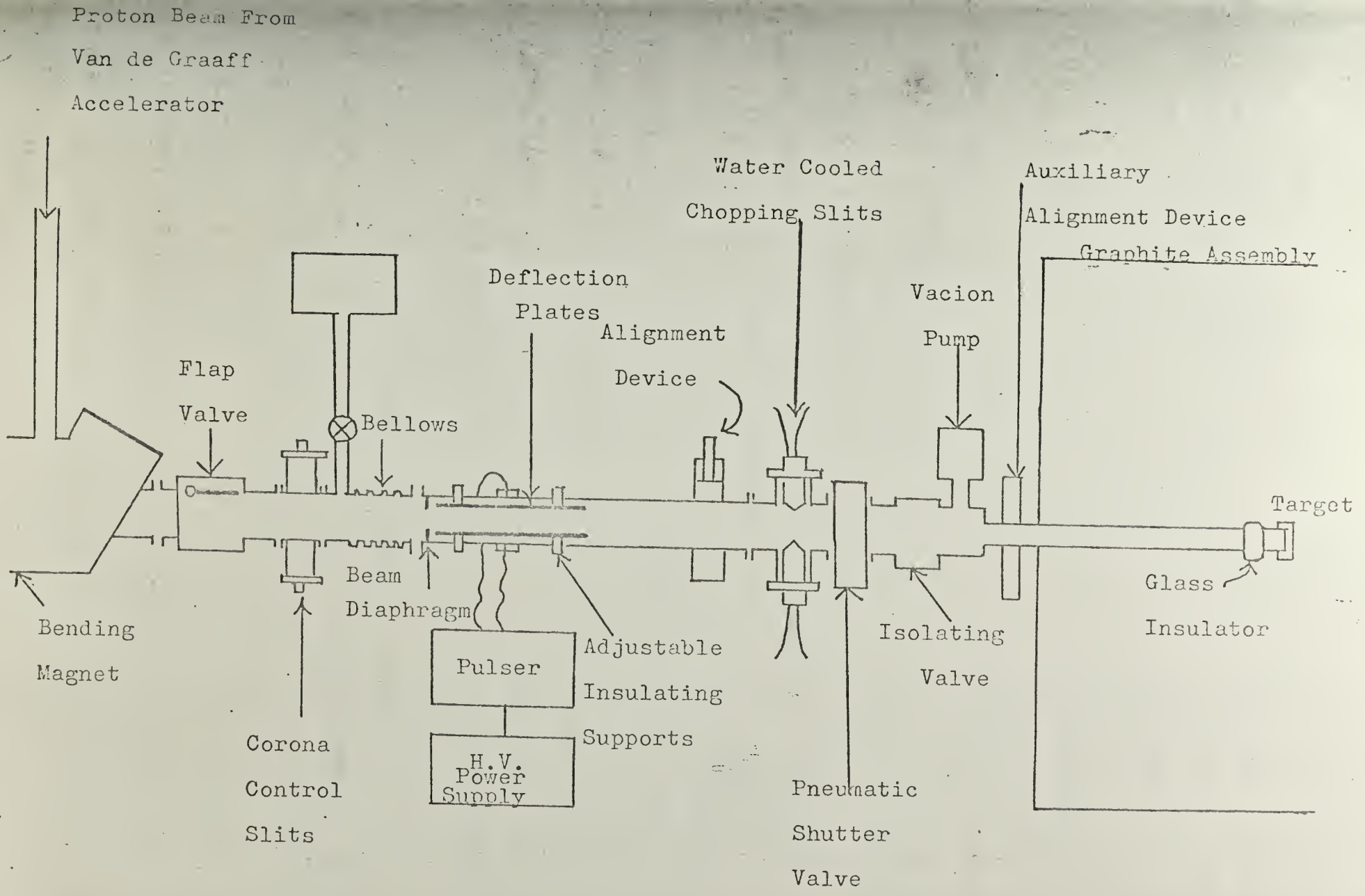

Figure 3.2 Plan View of the Experimental Installation

downward and bent into the horizontal beam tube by a bending and analyzing magnet. The beam tube was kept under a high vacuum by the diffusion pump of the accelerator, and by a small Vac Ion pump located close to the target.

The deflecting plates delivered a high voltage pulse which deflected the beam. The water-cooled chopping slits were mounted after the deflection plates for the purpose of intercepting the beam when it was swept off the target. The distance between the slits, the shape of the high voltage pulse, and the deflecting plates configuration determined the shape of the pulse reaching the target.

A remotely controlled pneumatic shutter valve was interposed between the chopping slits and the target. The beam could thus be cut off from the target, enabling work to be done around the assembly. The target tube itself was constructed of aluminum and was 23 inches long, 3/8 inch O.D., with a 1/16 inch wall thickness. The target assembly was located at the end of the target tube.

It was decided to cool the target in order to protect it from deterioration. This was done by sealing the end cap, which presses the target disc directly against the O-ring vacuum seal, with a plate into which short lengths of tubing had been brazed. (See Figure 3.3) Water forced through the cap removed the heat from the target disc.

3.3 The Neutron Source

As in previous experimental measurements of neutron

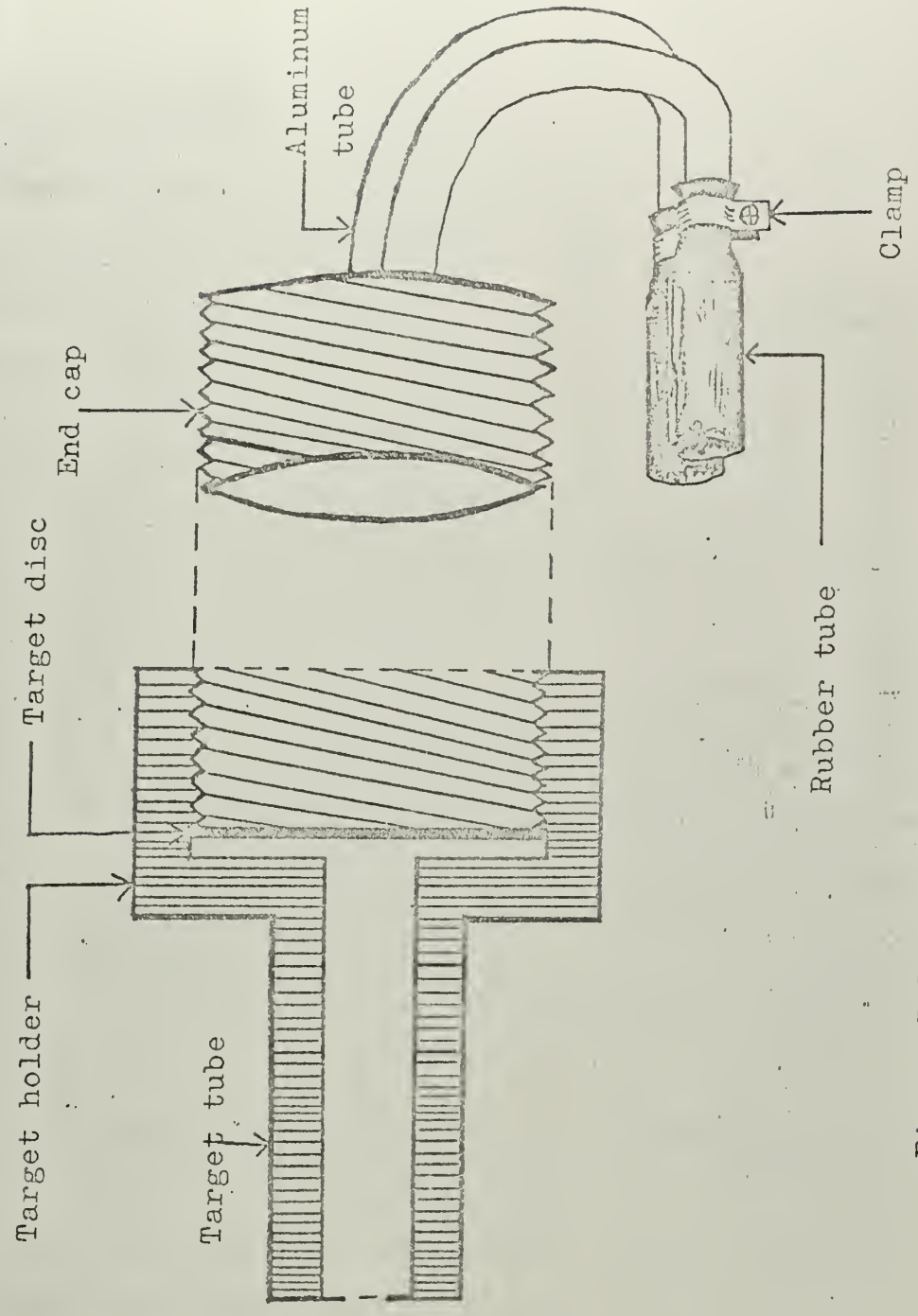

Figure 3.3 Target Cooling System

slowing down time (1,2), the $Li^7(p,n)Be^7$ reaction was used as the neutron source mainly on the basis of its high yield and relatively good homogeneity. For a given angle from the target and for laboratory proton energy up to 2.34 MeV, the reaction is monoenergetic. The threshold of the $Li^7(p,n)Be^{7*}$ reaction is shown in Figure 4.6 of Adamantiades' thesis. Because of neutron intensity considerations, a proton energy of 2.4 MeV was used in this experiment.

The target used in these experiments consisted of a layer of natural lithium 0.8/cm^2 thick deposited through evaporation on a circular tantalum disc 0.055 inches thick and 13/16 inch in diameter. Although the thickness of the target is less than 1/10 of the range of 2.5 MeV protons in lithium, some protons will undergo slowing down collisions before undergoing nuclear reactions. The energy spread of the actual beam of protons incident on the target, however, is very small in the Rockefeller Van de Graaff accelerator.

To summarize, there were three major sources of neutron energy inhomogeneity in this experiment:

1) Angular dependence of neutron energy.

2) Excited product nucleus reaction.

3) Energy spread of the reacting protons.

As mentioned in section 2.1, this energy inhomogeneity could be tolerated since the slowing down time is relatively insensitive to the source energy.

3.4 The Moderating Assembly

The moderating assembly (see Figure 3.4) consisted of reactor-grade graphite stringers, approximately 4.0 inches by 4.25 inches and 4.0 feet long, stacked so that alternate layers were at right angles to each other. The overall dimensions of the assembly was 3.6 feet by 4.0 feet by 4.0 feet. The entire assembly was covered with aluminum foil to shield the monitoring and detection systems from R.F. pickup coming from the pulsing system, although this pickup was never entirely eliminated.

In a stringer located at the center of one face of the pile, a hole was bored so that the target, along with the cooling water tubes and the cables of the monitoring system, could be inserted into the center of the assembly.

At a right angle to, and on the same horizontal plane as the beam tube was an open channel, 4.0 inches wide, 4.25 inches high, and 19.3 inches long, which led from the target to one face of the assembly. It was through this channel that the detector, foil, and graphite spacers were inserted or removed (see Section 4.2).

3.5 Electronic Systems

3.5.1 Beam Pulsing System

Although the Rockefeller accelerator has a terminal pulsing capability, its single sweeping frequency was much too high for this experiment. Therefore, a post-acceleration system was used which had the advantage of a variable

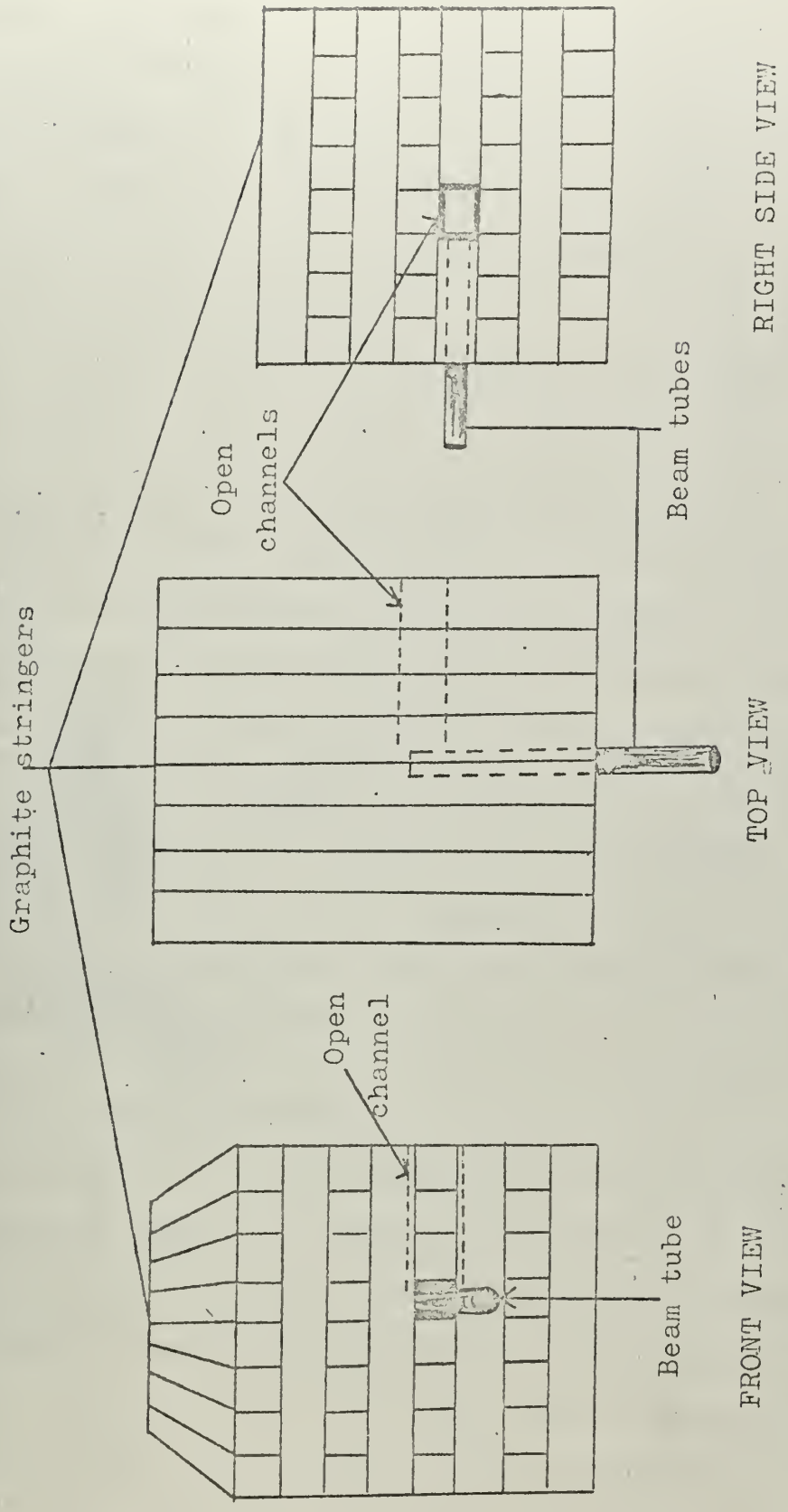

Figure 3.4 Moderating Assembly

pulse width and repetition rate (see Figure 3.5). A detailed discussion of the system is given in Reference (1). A repetition rate of 2kc/sec was used, allowing 500 μsec between pulses, which was enough time to allow all transient neutron levels to die out. A pulse width of 200 nsec was used in this experiment.

The pulsing system was triggered by the General Radio wave generator (type no. 1217-A), which was also used to start the timing circuits of the analyzing system (see Section 3.5.3). The output pulse of the G.R. pulser triggered an E-H Research Laboratories Model No. 130 pulser.

The variable width output pulse of the E-H pulser was the input for the driver circuit which is essentially a pulse amplifier. An extensive discussion of the driver circuit is given by A.E. Waltar (3), who designed it. Vaughan modified the circuit somewhat to give a narrower pulse. In this experiment the driver circuit delivered a 2.9 KeV pulse to the deflection plates.

3.5.2 The Detection System

The object of these experiments was to detect neutron capture gamma rays as a function of time, so an efficient gamma-ray detector was required. A Harshaw Integral Line Scintillator Assembly, consisting of a 3 inch x 3 inch NaI(Tl) crystal attached to a 6363 DuMont photomutiplier tube, was used. The crystal and tube are hermetrically sealed within an aluminum housing, making the detector

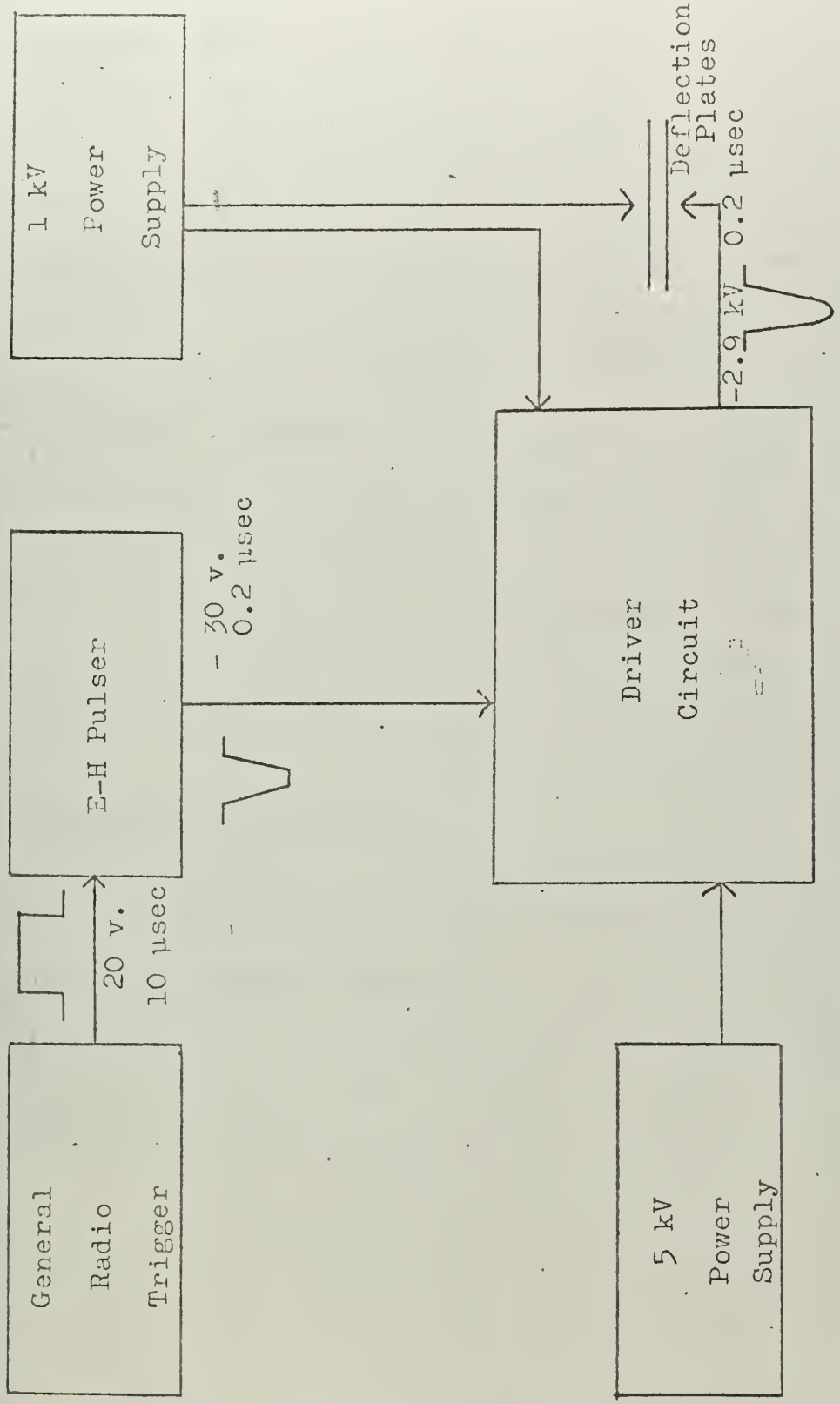

Figure 3.5 Block Diagram of Pulsing System

a simple plug-in unit. A thermal neutron shield, consisting of 3 mm. thick boron carbide enclosed by aluminum, was provided to keep activation of the sodium at a minimum.

The solid state preamplifier, which plugged into the end of the detector assembly, was designed and built in a cylindrical can having the same diameter as the detector. Vaughan gives a schematic diagram of the preamplifier in Figure 4.6 of his thesis.

The high voltage for the phototube was provided by a 2 KV power supply, while the preamplifier was powered by a small solid state power supply. The entire detector was wrapped in aluminum foil, and all leads to and from the detector were enclosed within copper braid to eliminate R.F. pickup.

3.5.3 The Analyzing System

The main features of the time analyzing system were:

1) A start pulse providing a time reference, derived from the beam pulsing network.

2) A stop pulse indicating the time at which an event of interest took place, derived from the detector.

3) A timing unit, used in conjunction with a multichannel analyzer, which produced a count in the channel corresponding to the time interval between the arrival of the start and stop pulses. Conventional, commercially available equipment was used in the entire analyzing system (see Figure 3.6).

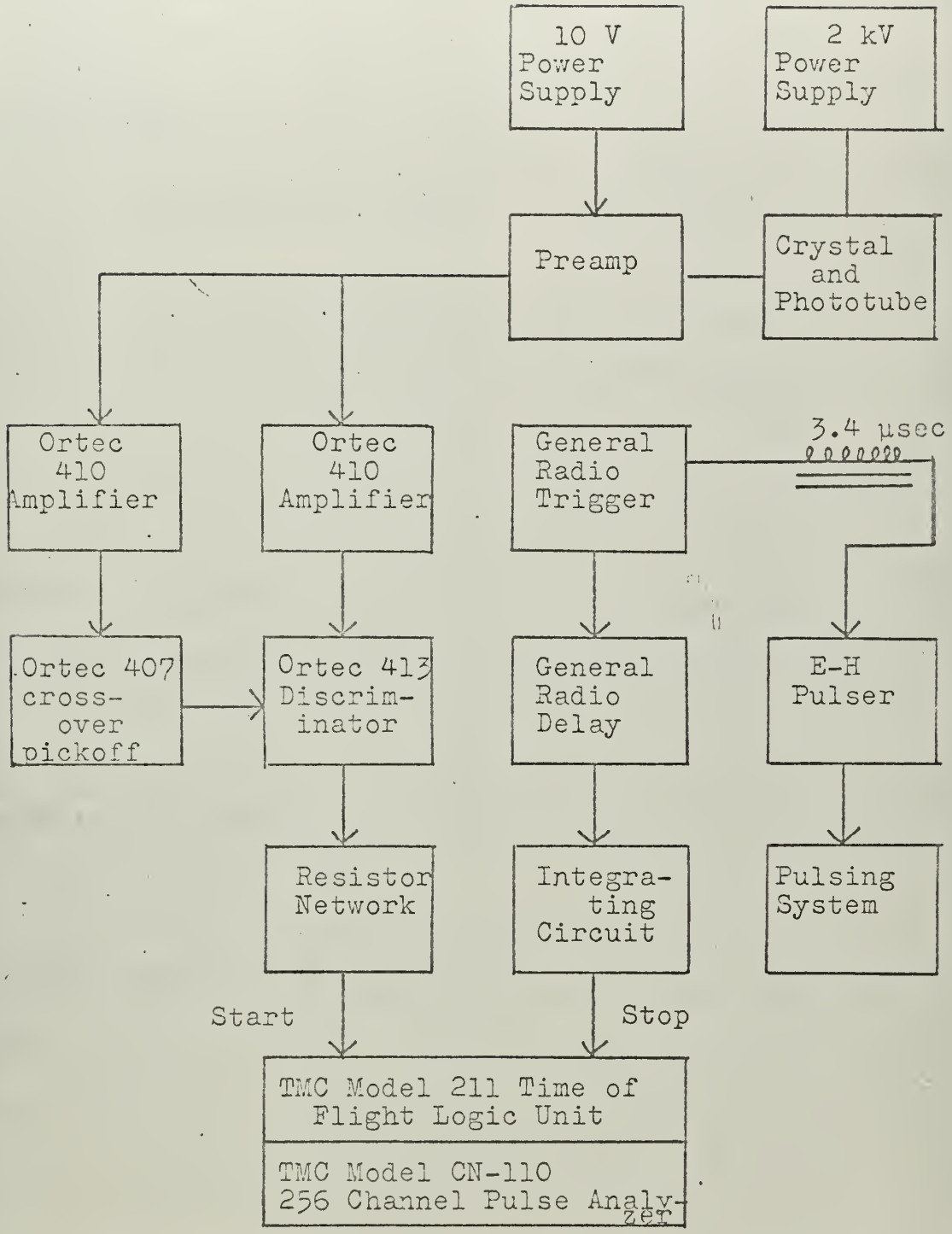

Figure 3.6 Analyzing System

The start pulse was obtained from the General Radio trigger (see Section 3.5.1). This pulse was fed through a General Radio 1392-A Time Delay Generator which provided a stable, variable time delay. Unfortunately, the output pulse of the G.R. delay was too narrow to trigger the timing unit; and an integrating circuit was employed to stretch the pulse.

The detector output signal was fed to two Ortec 410 Strobbed Discriminator, with the strobe input coming from an Ortec 407 Zero Cross-over Pickoff Unit. The cross-over pickoff was fed by the other Ortec 410, whose time constants had been optimized for a stable cross-over point. A positive logic signal was provided by the discriminator when the incoming detector signal met minimum energy requirements. The strobe assured a constant time relation between the detector input and discriminator output. The positive logic pulse was attenuated by a resistor network before it was fed into the timing unit.

The timing unit consisted of a TMC Model 211 Time of Flight Logic Unit which plugged into the TMC Model CN-110 256 Channel Pulse Analyzer. The 211 unit converted the time difference between the trigger input and a detector signal to an appropriate channel number, depending on the scale factor which could be varied from 0.25 to 64 μsec/channel. This information was then stored in the multi-channel analyzer.

The TMC 211 Unit could handle more than one stop pulse

(detector signal) per cycle. However, 16 μsec were needed to analyze and record each incoming signal. A correction for this deadtime was included in the computer program used to process the data (see Section 4.3). More detailed information on the 211 unit and the multi-channel analyzer is given in Reference (4).

3.5.4 The Monitoring and Normalizing System

To insure that the pulsing system was operating under the best possible conditions at all times a beam pulse monitor was provided.

The beam pulse monitor was necessary due to the problem of focusing the proton beam from the accelerator. Because of various changes and drifts in the accelerator, the setting for optimum focusing changed from day to day, and had to be constantly adjusted. In pulsed operation, the only practical method of focusing was to use an electrical signal from the target itself and to observe the signal with a fast oscilloscope. The system employed is sketched in Figure 3.7. Notice that the target was insulated from the beam tube with a glass ring which enables the signal to be picked off the target. The monitoring system was especially susceptible to R.F. pick-up from the pulser. All cables of the system were shielded against pick-up; but the problem was never completely eliminated. A typical target pulse can be seen in Figure 4.11 of Vaughan's thesis. The electronic pulse being delivered to the deflection plates

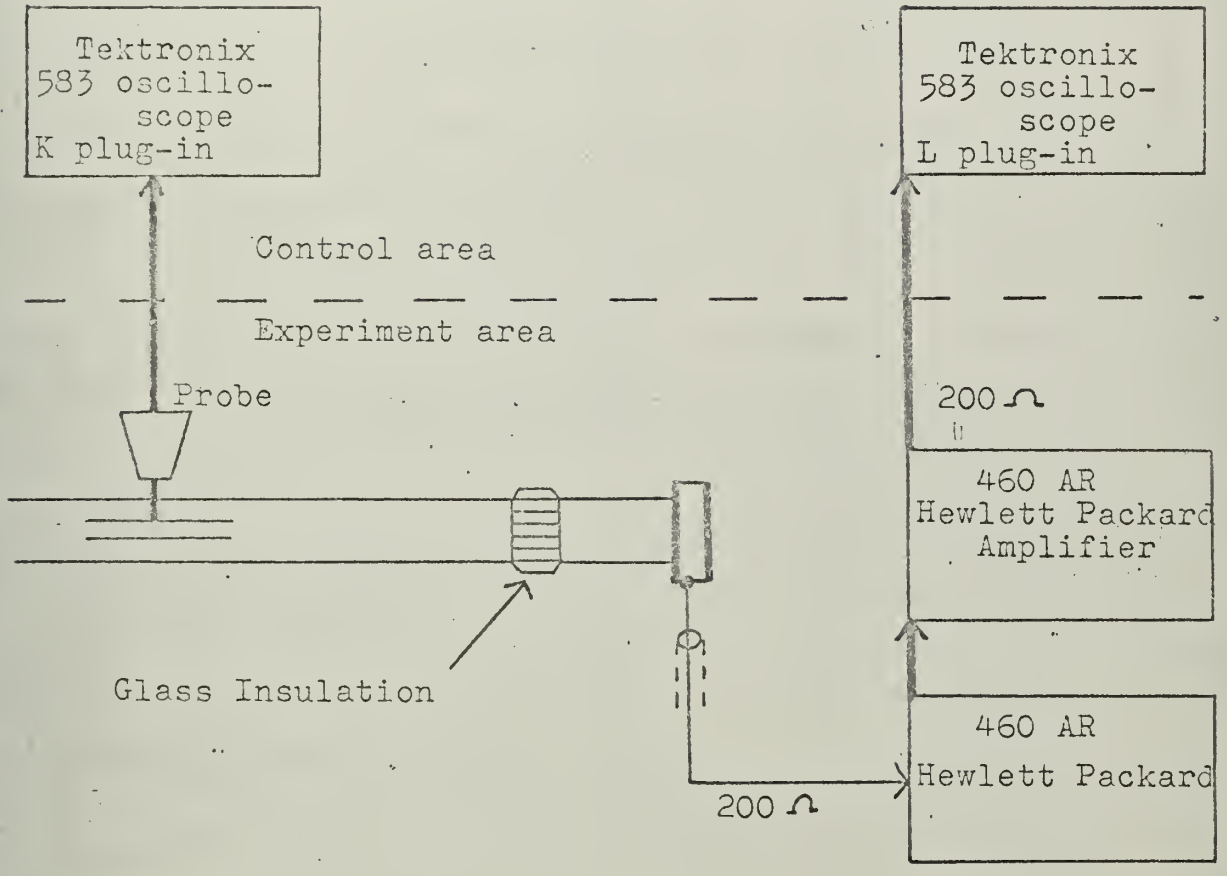

Figure 3.7 The Monitoring Systems

could also be monitored. This system is also shown in Figure 3.7.

A neutron monitor was used as a means of normalization for comparing different runs and subtracting background. A detailed discussion of normalization is given in Chapter 5 of Reference (1). As in previous experiments, this author concluded that total neutrons produced during an experiment would be the most reliable quantity to use of normalization. A boron triflouride counter was placed between the graphite stringers of the assembly about 13 inches from the target and on the side opposite the absorber foil and detector. Thus, with the output of the BF_3 tube going to a scaler, the time integrated neutron flux as seen by the detector could be recorded.

References for Chapter 3

1. A.G. Adamantiades, Ph.D. Thesis, Department of Nuclear Engineering M.I.T., (1966).

2. J.E. Vaughan, M.S. Thesis, Department of Nuclear Engineering M.I.T., (1967).

3. A.E. Waltar, S.M. Thesis, M.I.T., Department of Nuclear Engineering, (1962).

4. Transistorized Multi-Channel Pulse Analyzer System Model CN-110, Technical Measurement Corporation, North Haven, Connecticut.

CHAPTER 4

Experimental Results and Discussion

4.1 The Use of Resonance Absorbers as Neutron Density Indicators

Resonance absorbers were used in this experiment to sample neutron population at the resonance energy. The most suitable materials for this purpose are those which exhibit a strong isolated absorption resonance. The higher and narrower the resonance, the better it approximates a delta function. Table II of Reference (1) gives a list of absorbers which exhibit strong isolated resonances. The energy and peak cross section of the resonance is also given.

Another important consideration in choosing a suitable absorber was its prompt neutron capture gamma-ray spectrum. This did not prove to be a problem since the de-excitation gamma rays of most materials are spread over a wide range of energy. Reference (1) gives capture gamma-ray spectra for the three absorbers used in these experiments: cadmium, indium, and gold. The capture gamma spectra of these materials extends from the KeV region to energies exceeding 7 MeV.

Indium and gold were chosen for their strong isolated resonances at 1.46 eV and 5.0 eV respectively. Cadmium,

which has a broad resonance that reaches a maximum at about 0.2 eV, was also used, although it was expected that the time resolution for these measurements would not be as good as that for indium and gold.

4.2 Performance of the Experiment

In order to insure a constant geometric relationship between the foil and detector, a foil holder was used. The foil holder consisted of a one inch thick slab of graphite, which was sized to fit into the channel of the assembly and was bonded to the end of the detector with epoxy cement. The foil was taped to this slab, and the whole detector-foil array was inserted into the graphite assembly through the channel (see Figure 4.1).

To measure the spatial dependence of the slowing down time, it was necessary to be able to move the detector-foil array along the channel. Graphite slabs of varying thickness, which were inserted in the channel between the source and foil, assured that there would always be solid moderating material in front of the foil.

Before performing the actual experiments, short runs were made while varying the discriminator of the Ortec 413 Strobbed Discriminator. For each foil, the discriminator setting which resulted in the best foil counts to background counts ratio was determined.

A typical set of experimental data is shown in Figure 4.2(a). These results are for a 7 cm x 7 cm x 0.05 cm gold

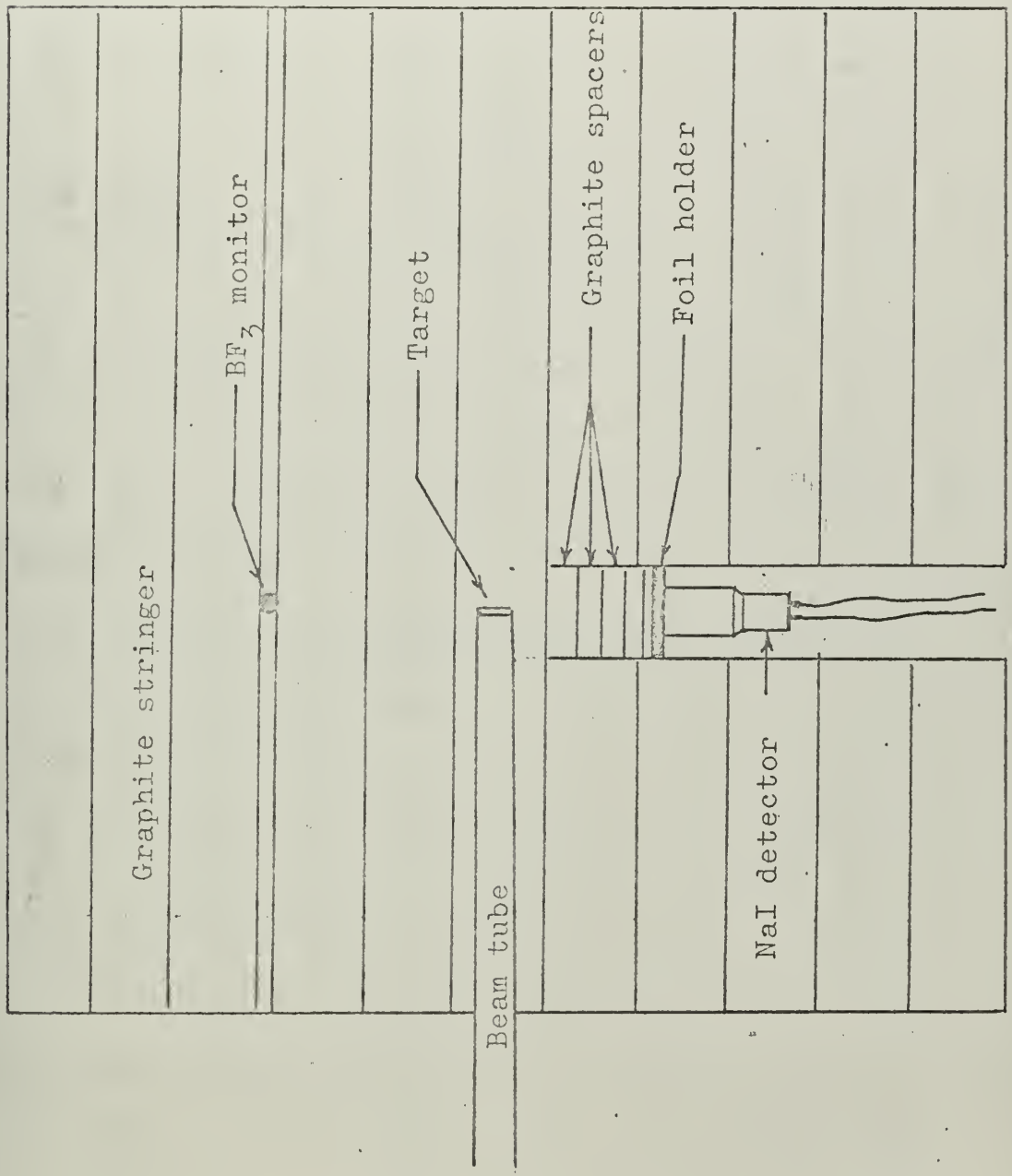

Figure 4.1 Horizontal Mid-Plane of Moderator Assembly

foil positioned 28 cm away from the target. The beam pulse width was 200 nsec, and the time interval between bursts was 500 μsec. The channel width was 250 nsec. A time distribution with the gold absorber in place was taken, and a distribution without the absorber was taken immediately afterwards. The BF_3 counts for the gold foil was 261,111 and for the background was 259,992. Notice the very prominent peak around channel 20. This peak is called the prompt peak and occurs when the burst of protons hits the lithium target. This peak was used as an accurate zero time reference in the experiment. The right half of the graph (notice the change of scale) shows the region in which the most probable slowing down time occurred. No peak is discernible from the raw data.

4.3 Normalization, Background Subtraction, Dead Time Correction and Smoothing

As mentioned in Section 3.5.4, the time integrated neutron flux, as derived from a BF_3 tube, was used for normalization. The number of BF_3 counts registered by the scaler was recorded for each experiment. A factor obtained by taking the ratio of background-run BF_3 counts to foil-run BF_3 counts was applied to the foil data.

In order to obtain the net effect of neutron captures in the foil, the counts originating from all other events must be subtracted when the time distribution is taken. These sources of parasitic gamma rays include:

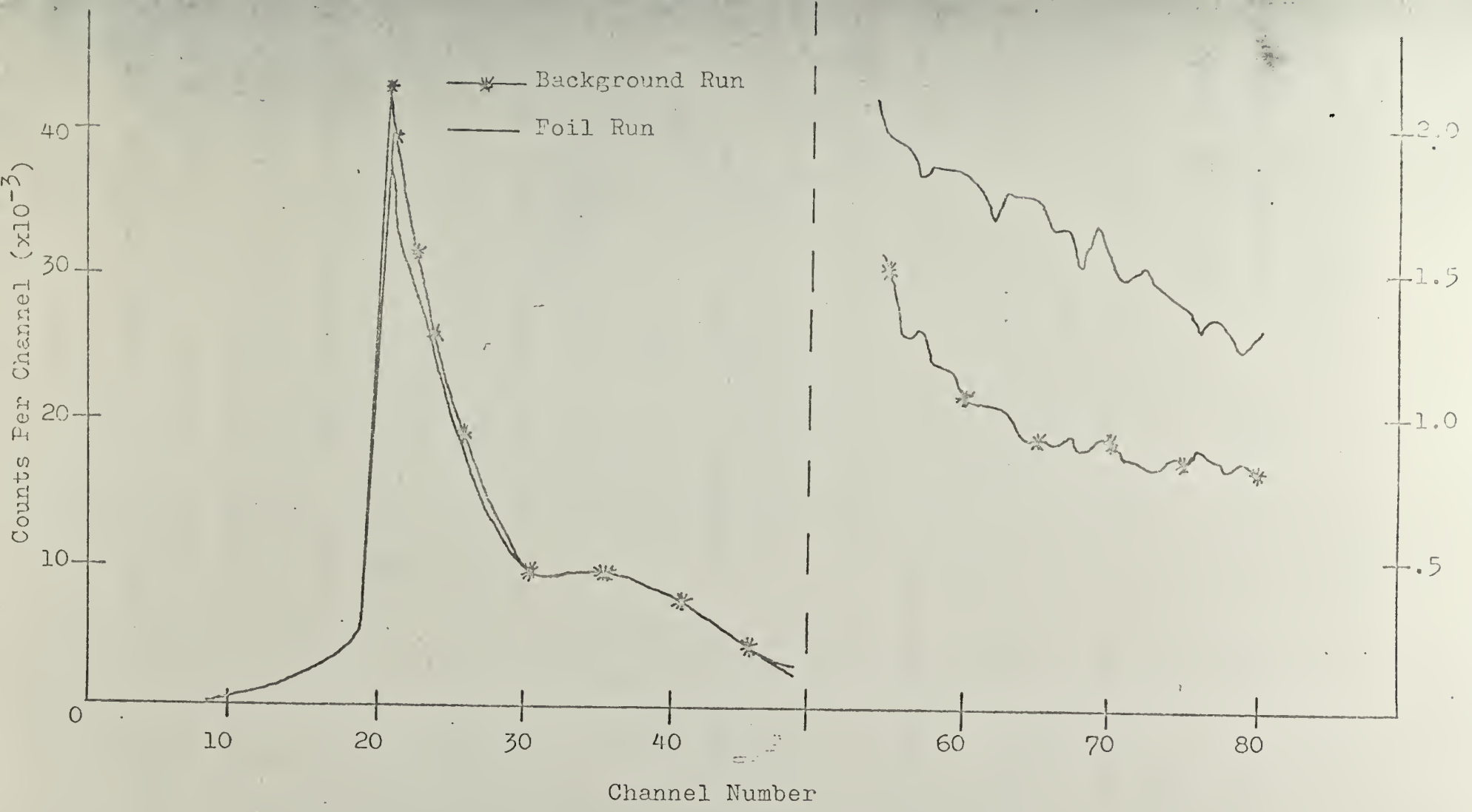

Figure 4.2 (a) Experimental Data From a Background and a Gold Foil Run

1) Inelastic scattering by the target, the absorber foil, and the detector.

2) Absorption in materials other than the absorber foil.

3) Reactions coincident with the neutron burst.

4) Overlapping events from preceding bursts.

5) Steady state background.

All these items were taken into account by taking a time distribution without the absorber foil in place, and then subtracting it from the distribution taken with the foil.

As mentioned in Section 3.5.3, there was a 16 μsec dead time associated with each count registered in the multi-channel analyzer. In Appendix C of Reference (2), a theoretical discussion of the dead time correction for the TMC Model 211 Unit is presented. The correction factors derived in that reference were used in this thesis.

Computer programs which normalized, subtracted the background, and applied dead time corrections to the raw data are listed in Appendix A.

Figure 4.2(b) shows the time distribution resulting from processing the raw data in Figure 4.2(a). It is obvious from this graph that there is a maximum in the time distribution occurring roughly at channel number 60. It is also obvious, however, that the fluctuations in the curve prevent an accurate determination of the maximum point. To reduce this uncertainty, a computer program

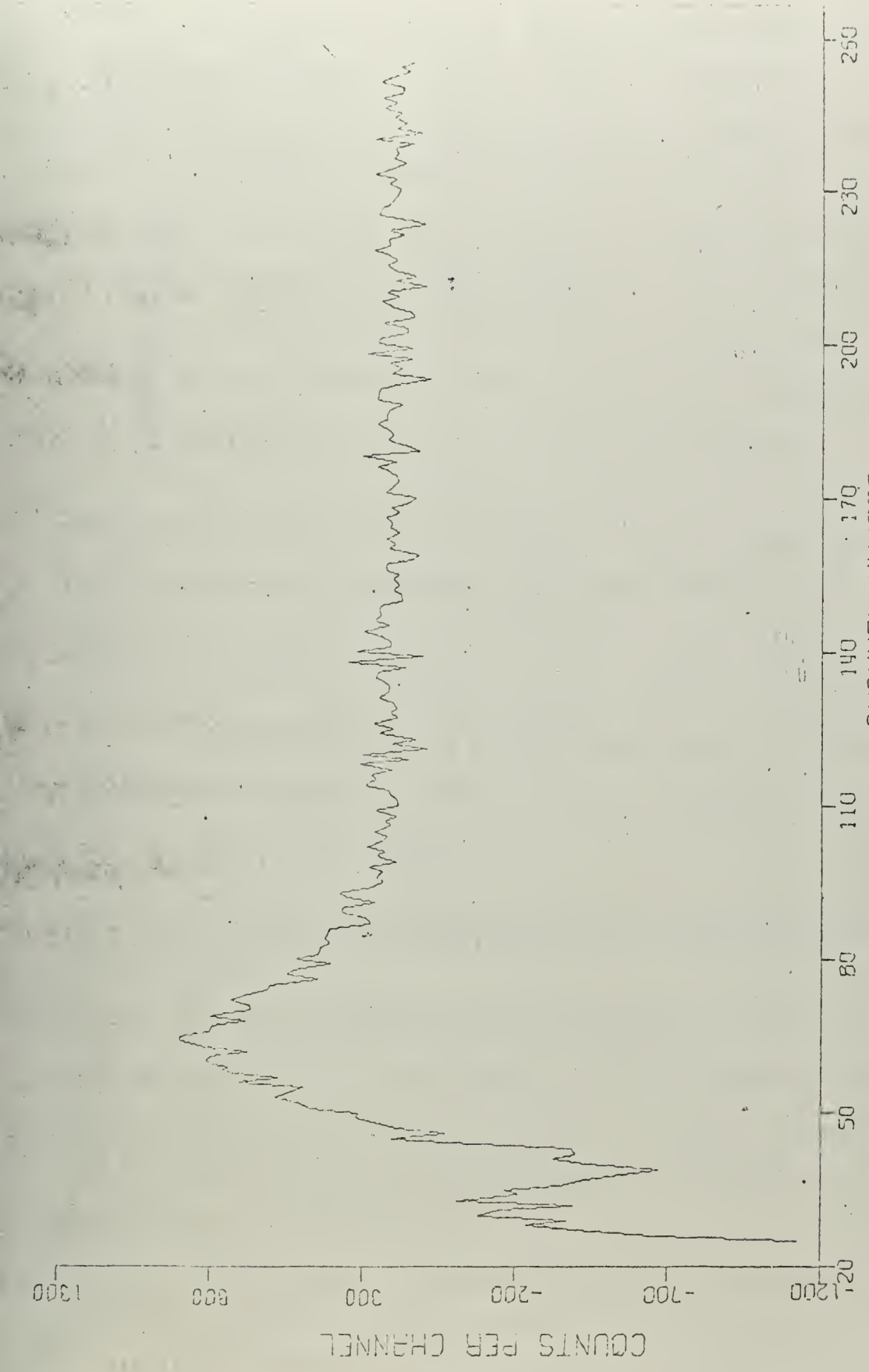

Figure 4.2 (b) Time Distribution at 5.0 eV and 28.00 cm Away From the Source

developed at M.I.T. (3) which applied a smoothing technique to the corrected data was used. Effectively, the program fits a Fouier series curve to the data points. Smoothing is accomplished by choosing not to fit the series to high frequency waves, which correspond here to statistical fluctuations. The frequency cutoff, above which all higher frequencies will be thrown away, is under the control of the programmer. Thus, any desired degree of smoothing can be effected to a set of data points. In this experiment, all frequencies less than four channels wide were dropped. Figure 4.2(c) is the smoothed version of Figure 4.2(b). Using this smoothed distribution; it was estimated that the maximum point of the time distribution occurred in channel 62.5±1. Since the prompt peak is in channel 20, the slowing down time is: (43.5±1) x (.25 μsec/channel) = 10.87±.25 μsec. The smoothing program is listed in Appendix A.

4.4 Space and Energy Dependent Slowing Down Time Measurements

If various absorbers with resonances located at different energies are used and if the distance of these absorbers from the source is varied, the time dependent neutron distribution can be measured as a function of space and neutron energy.

Figures 4.3 to 4.6 represent time distributions to the cadmium resonance; Figures 4.7 to 4.11 represent time

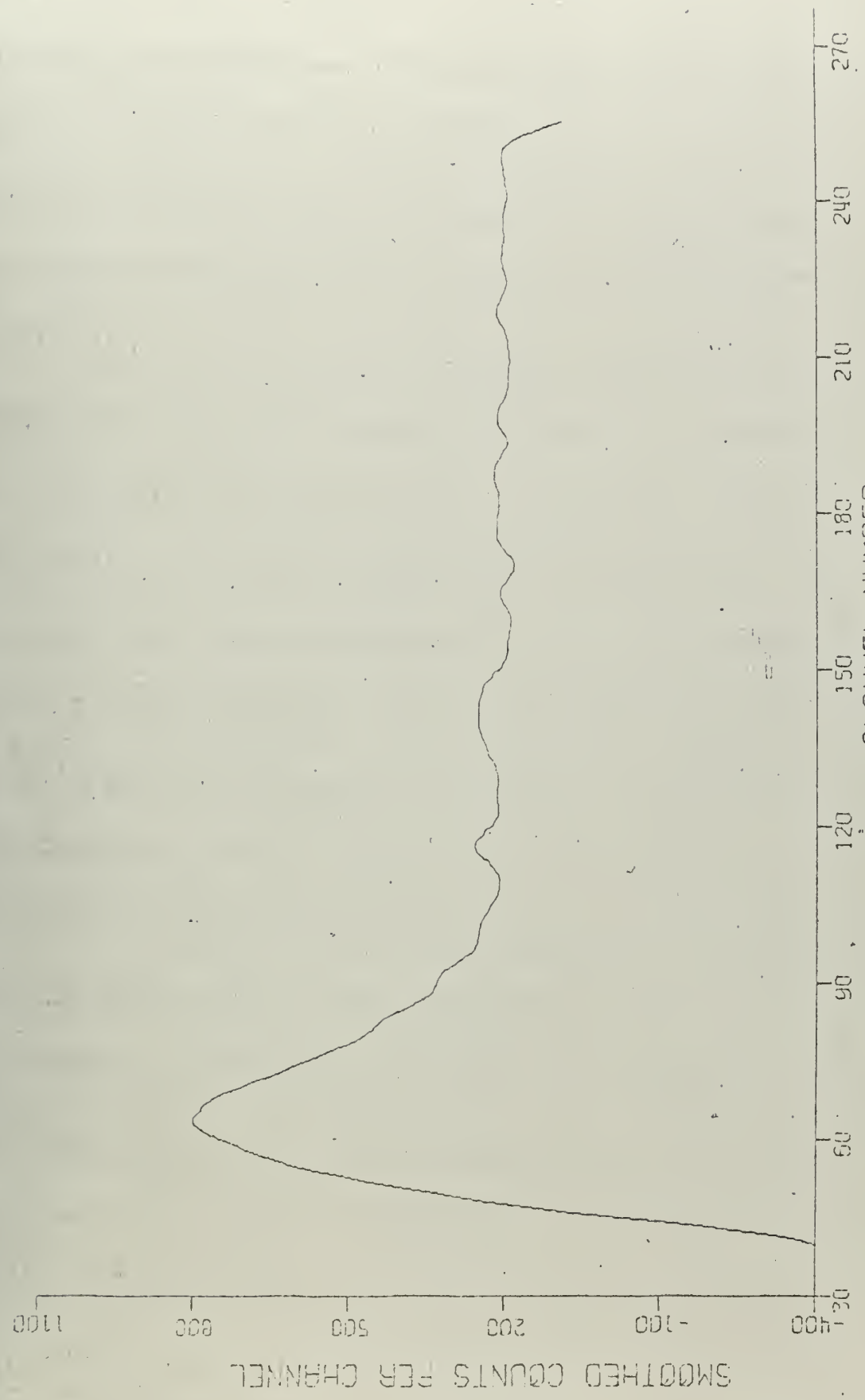

Figure 4.2 (c) Smoothed Version of Figure 4.2 (b)

distribution to the indium resonance; and Figures 4.13 to 4.16 represent time distributions to the gold resonance. In each Figure, (a) represents the distribution before smoothing and (b) after smoothing. Notice that the scale for the cadmium curves is 500 nsec/channel, while it is 250 nsec/channel for the indium and gold curves.

The results of this experiment, together with their probable errors, are graphically presented in Figures 4.17 to 4.19. The experimental uncertainty associated with each point reflects the broadness in the time distribution around the maximum value. As expected, the peaks of the cadmium distribution were much broader than those of gold or indium. The solid line in the gold and indium figures has been constructed from theoretical time distributions (see Section 2.3), based on diffusion theory (4).

The experimental results for the slowing down time to 5.0 eV appear to be in good agreement with the theoretical calculations. The agreement with theory for 1.46 eV is not as good. The experimental results indicate that there is little, if any, spatial dependence of the slowing down time for distances closer than about 30 cm from the source. For distances greater than 30 cm, the experimental results show a sharp rise in t_m with distance, indicating a strong spatial dependence. Theoretical calculations do not predict as sharp a rise of

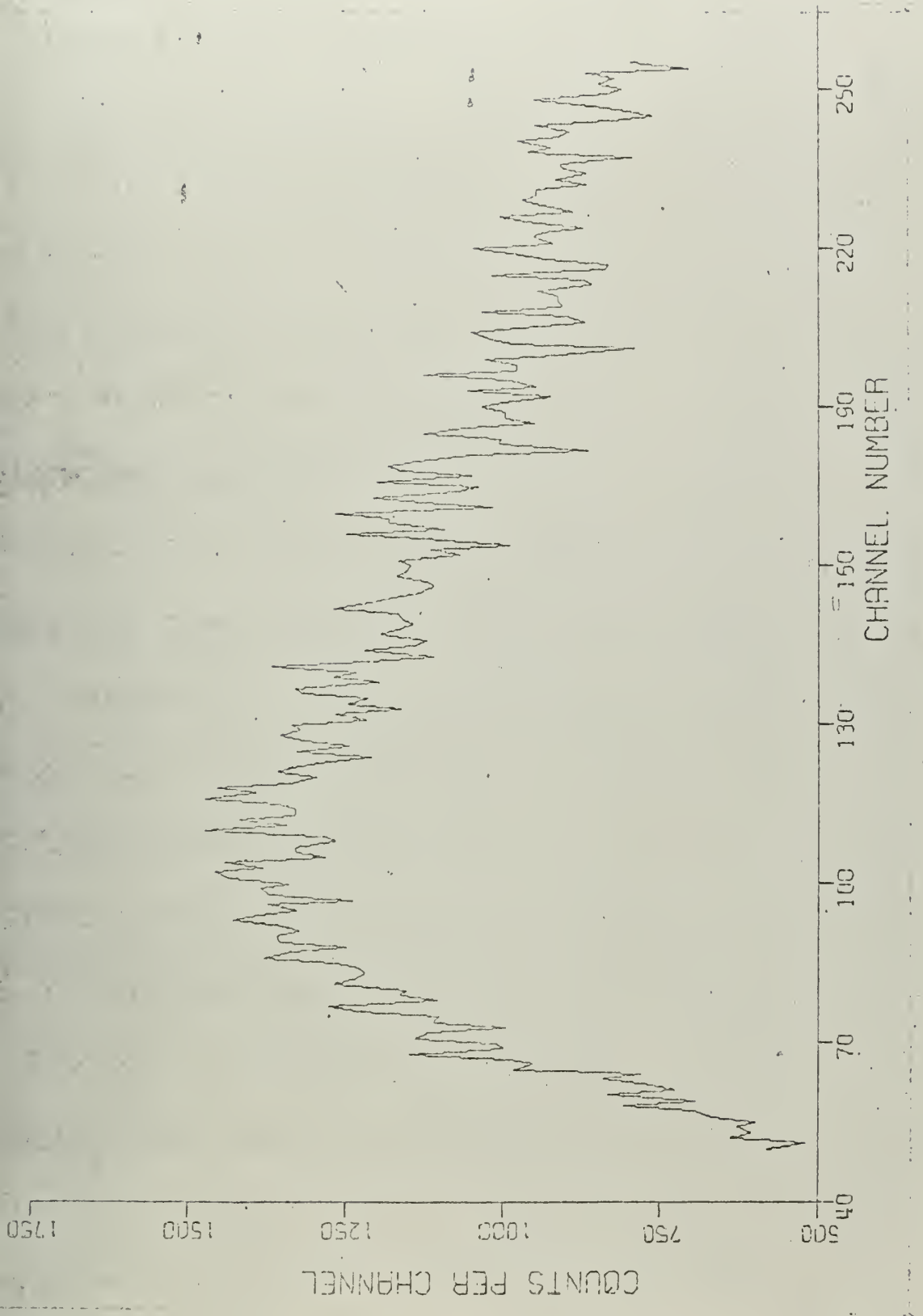

Figure 4.3 (a) Time Distribution at 0.2 eV and 12.5 cm Away From the Source

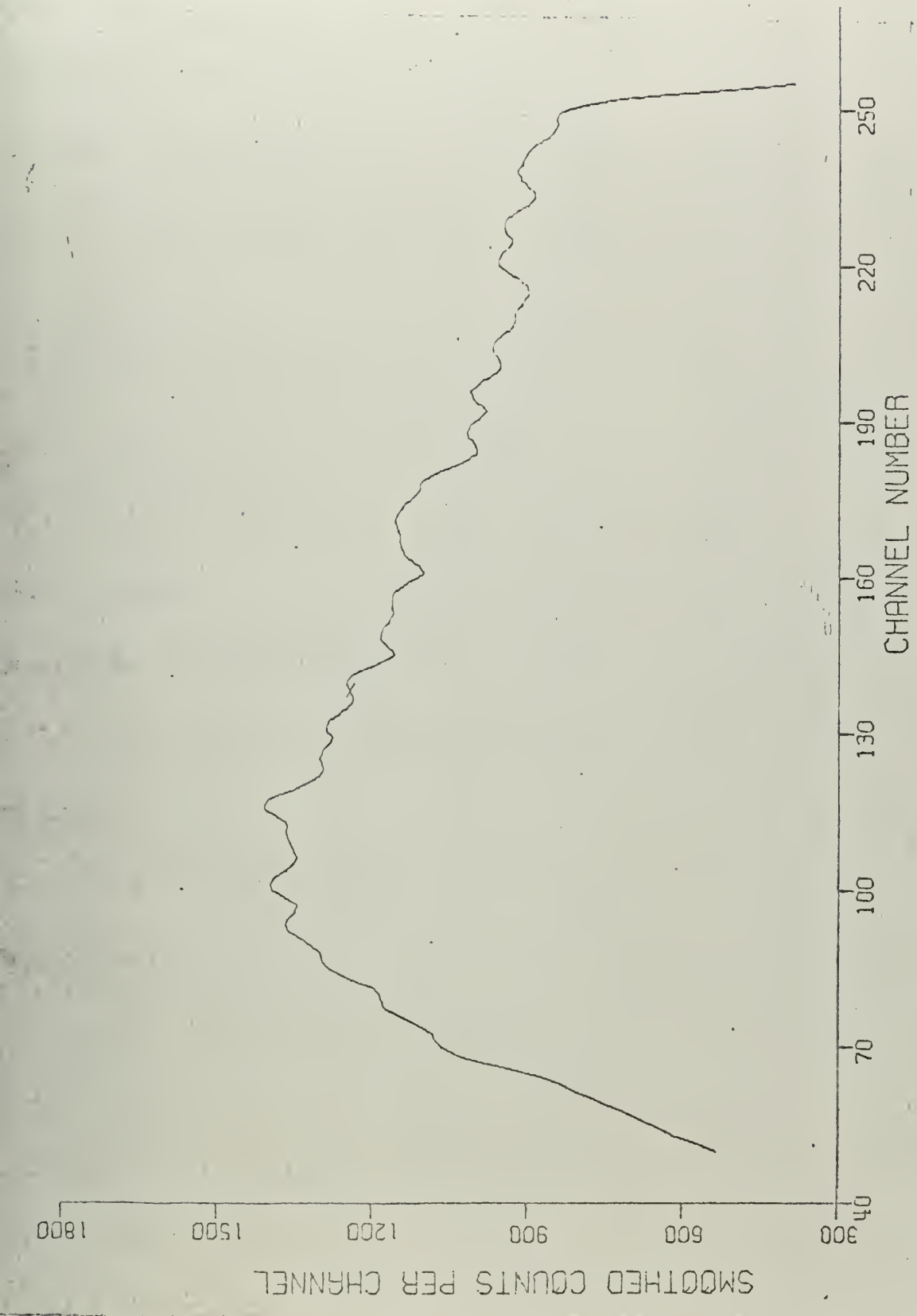

Figure 4.3 (b) Smoothed Version of Figure 4.3 (a)

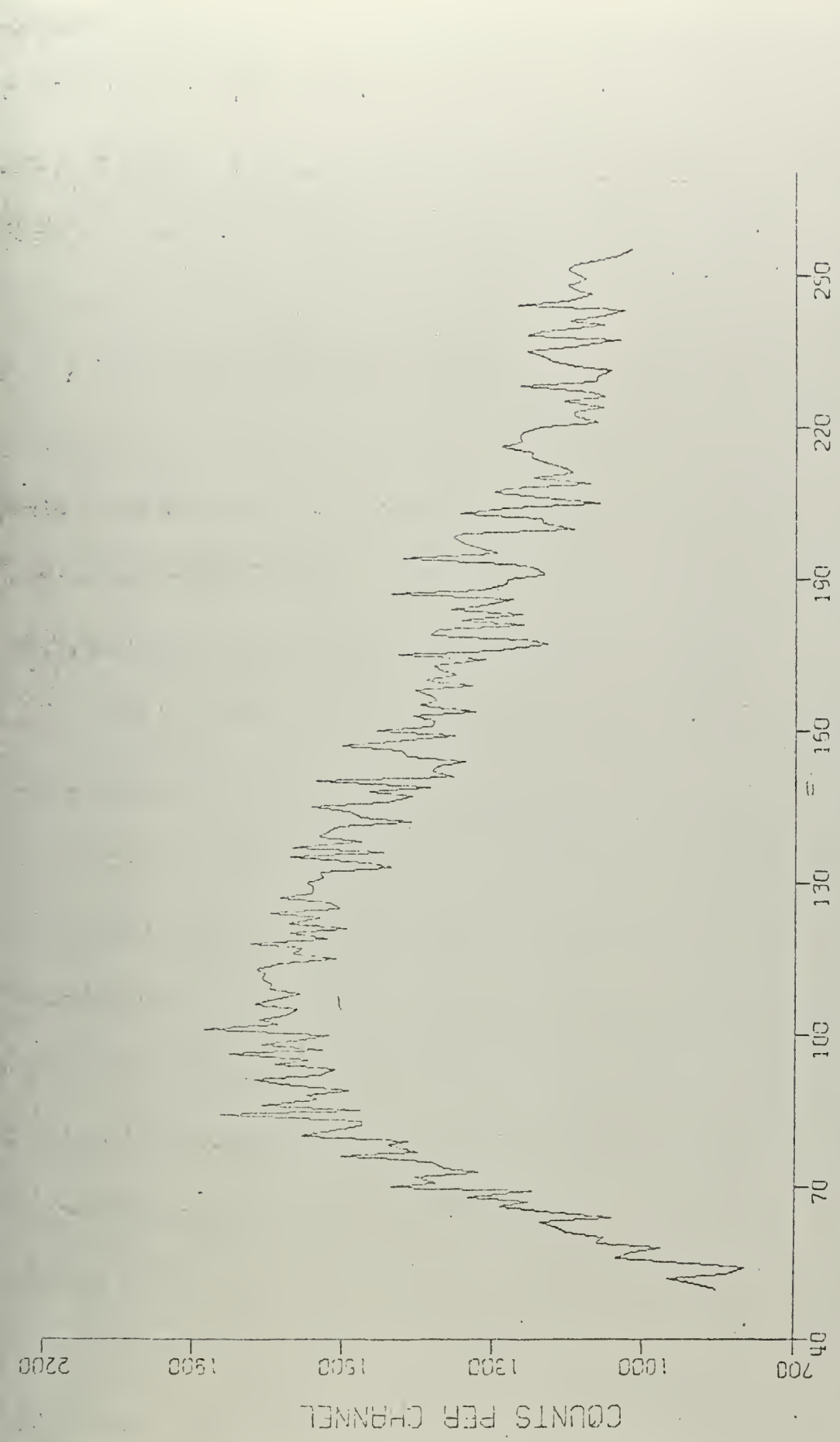

Figure 4.4 (a) Time Distribution at 0.2 eV and 18.0 cm Away From the Source

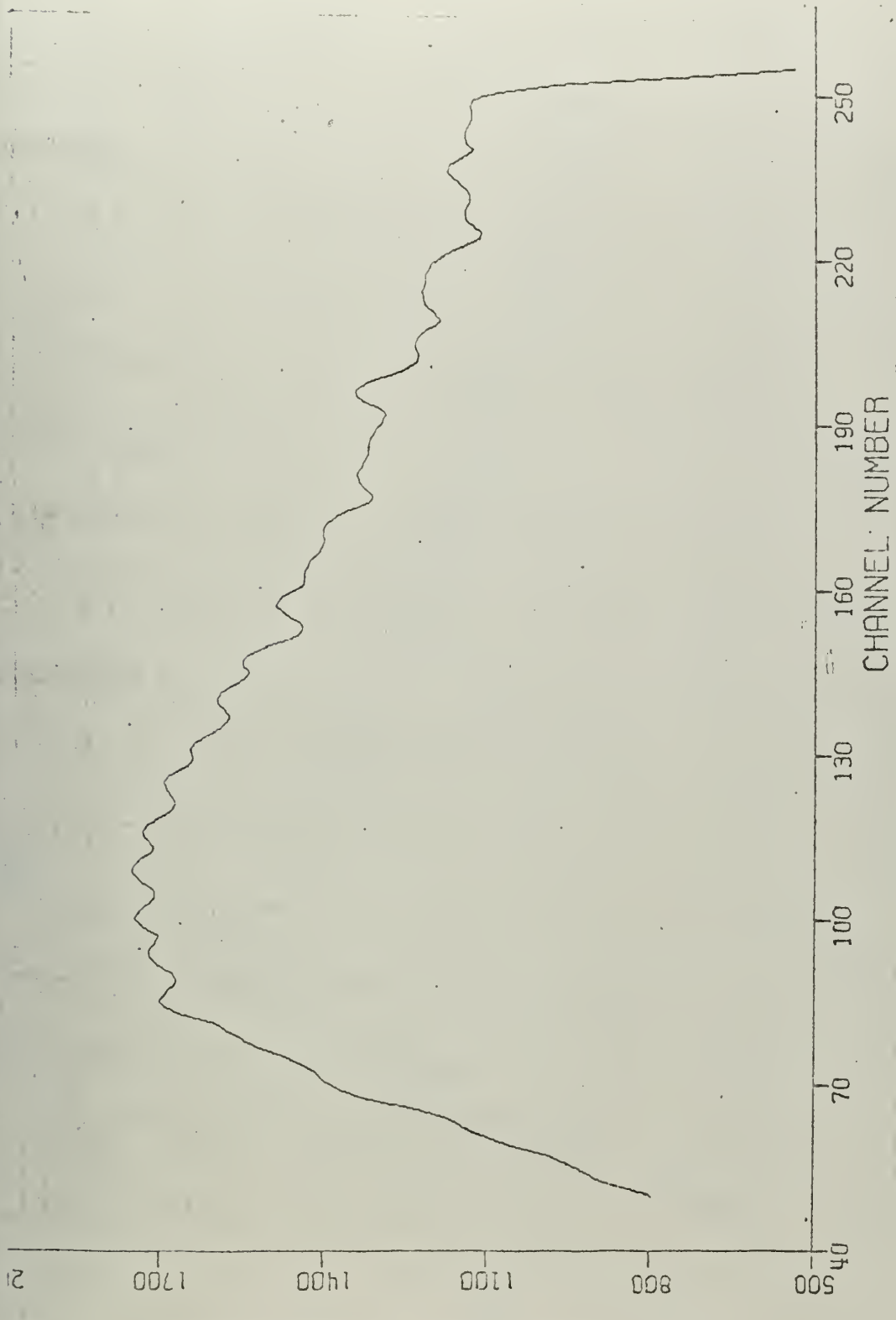

Figure 4.4 (b) Smoothed Version of Figure 4.4 (a)

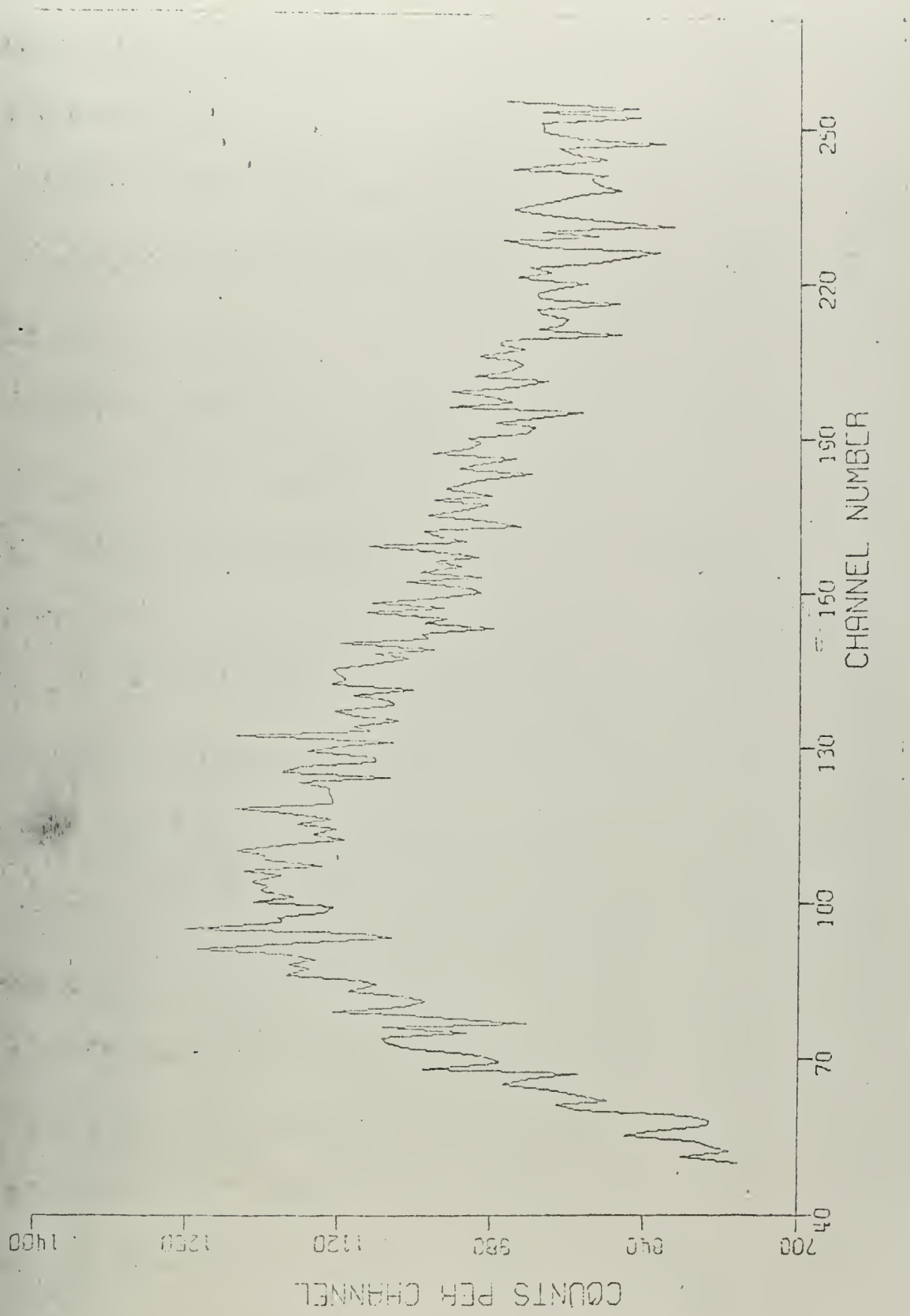

Figure 4.5 (a) Time Distribution at 0.2 eV and 28.0 cm Away From the Source

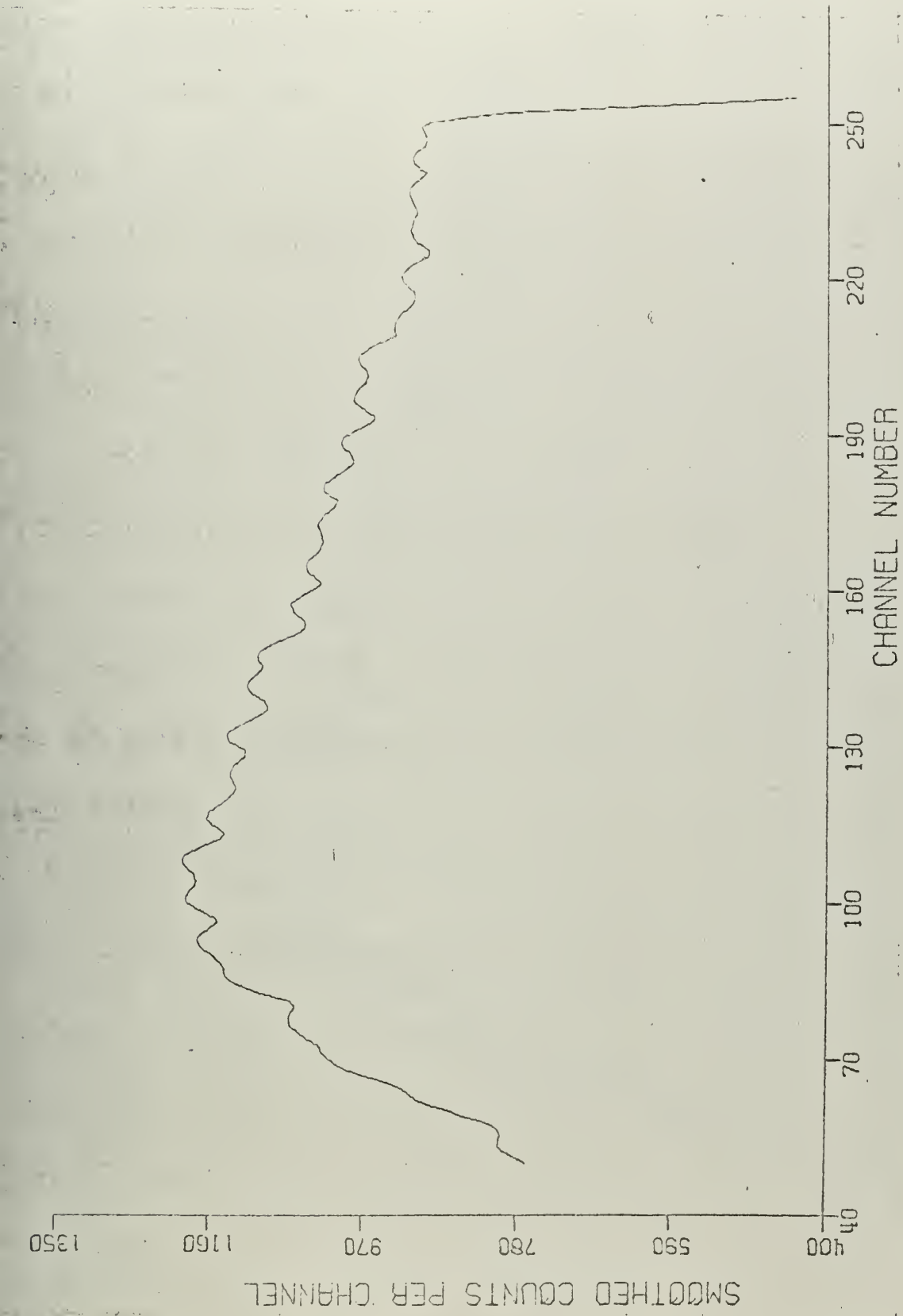

Figure 4.5 (b) Smoothed Version of Figure 4.5 (a)

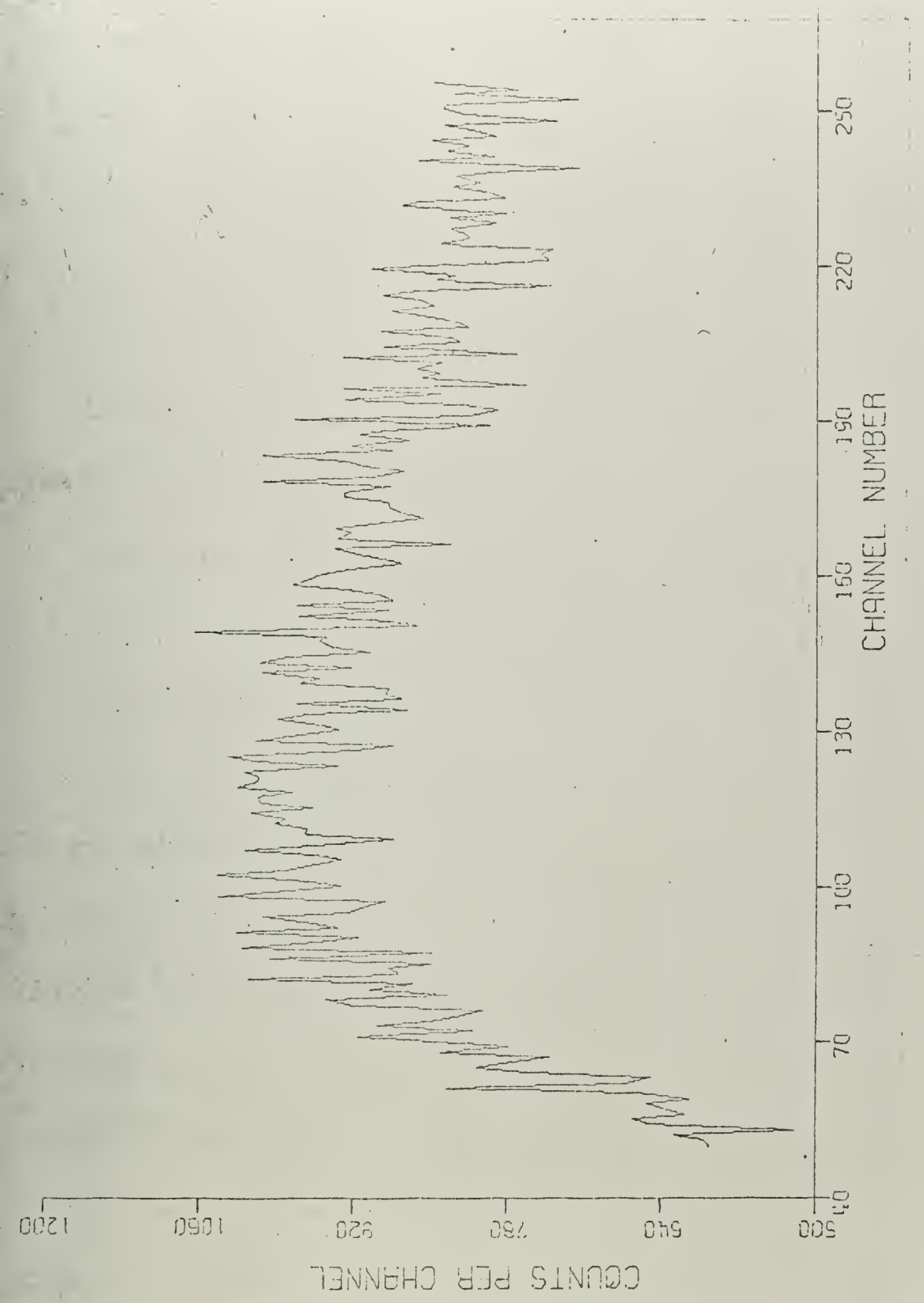

Figure 4.6 (a) Time Distribution at 0.2 eV and 44.5 cm Away From the Source

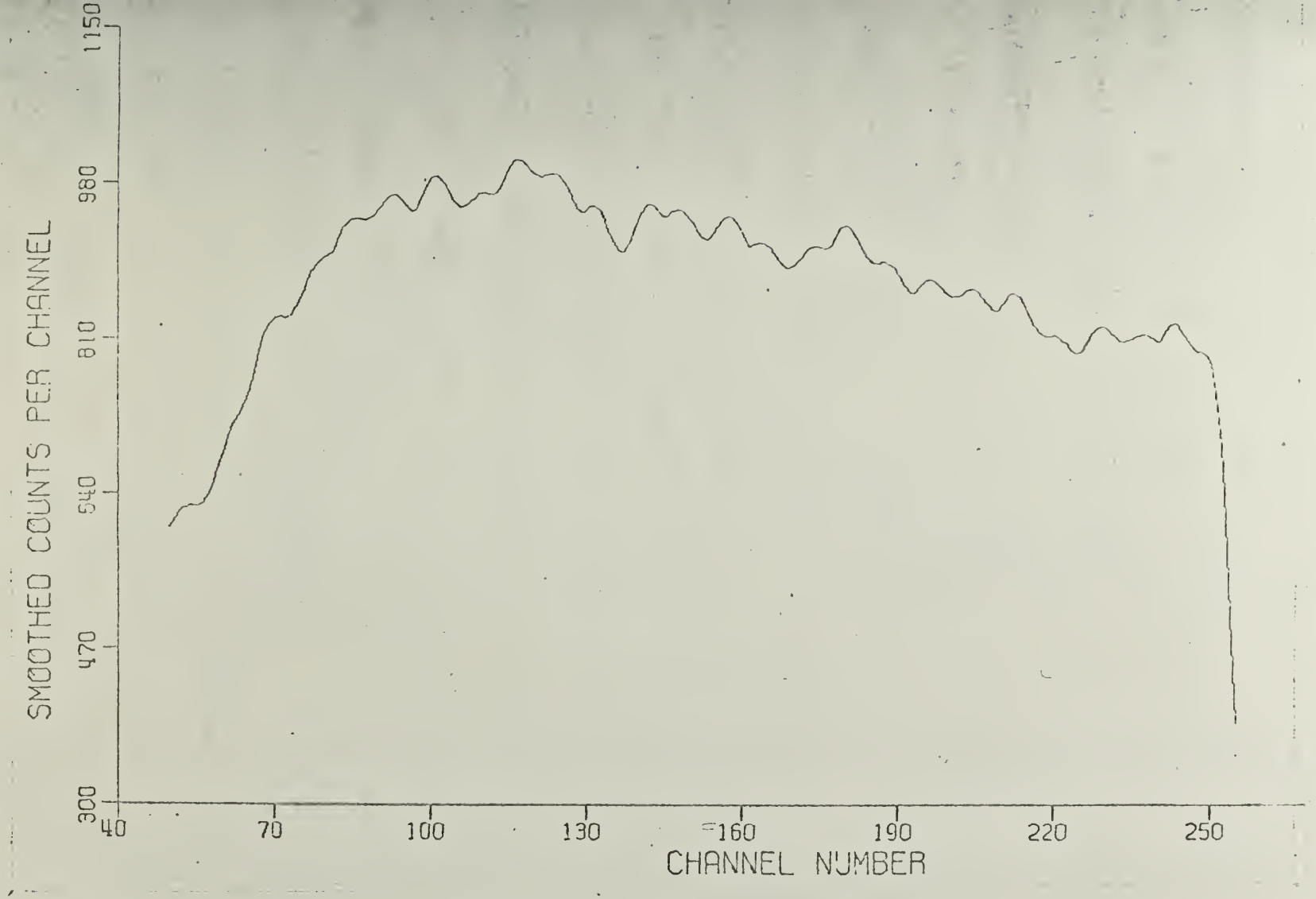

Figure 4.6 (b) Smoothed Version of Figure 4.6 (a)

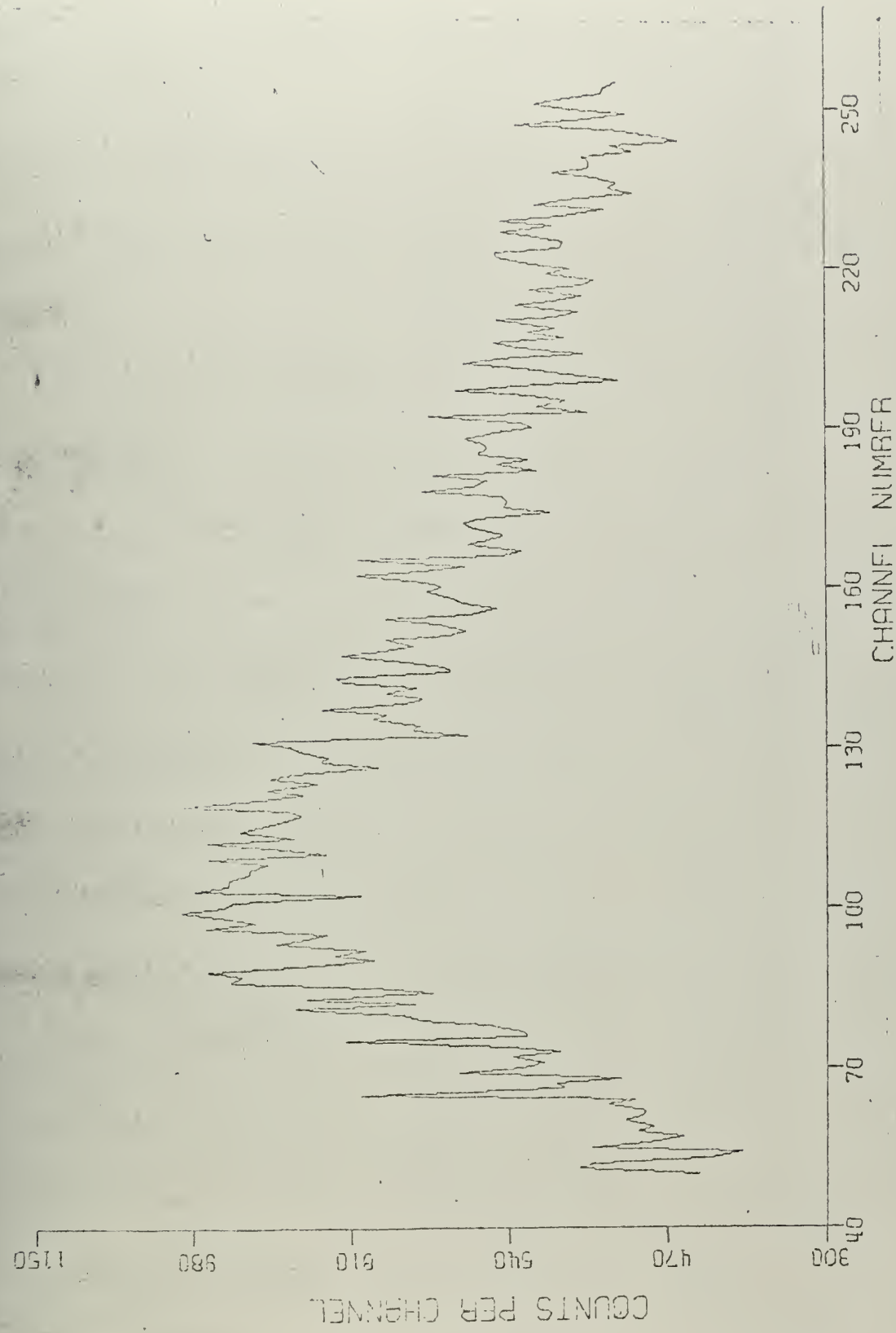

Figure 4.7 (a) Time Distribution at 1.46 eV and 12.5 cm Away From the Source

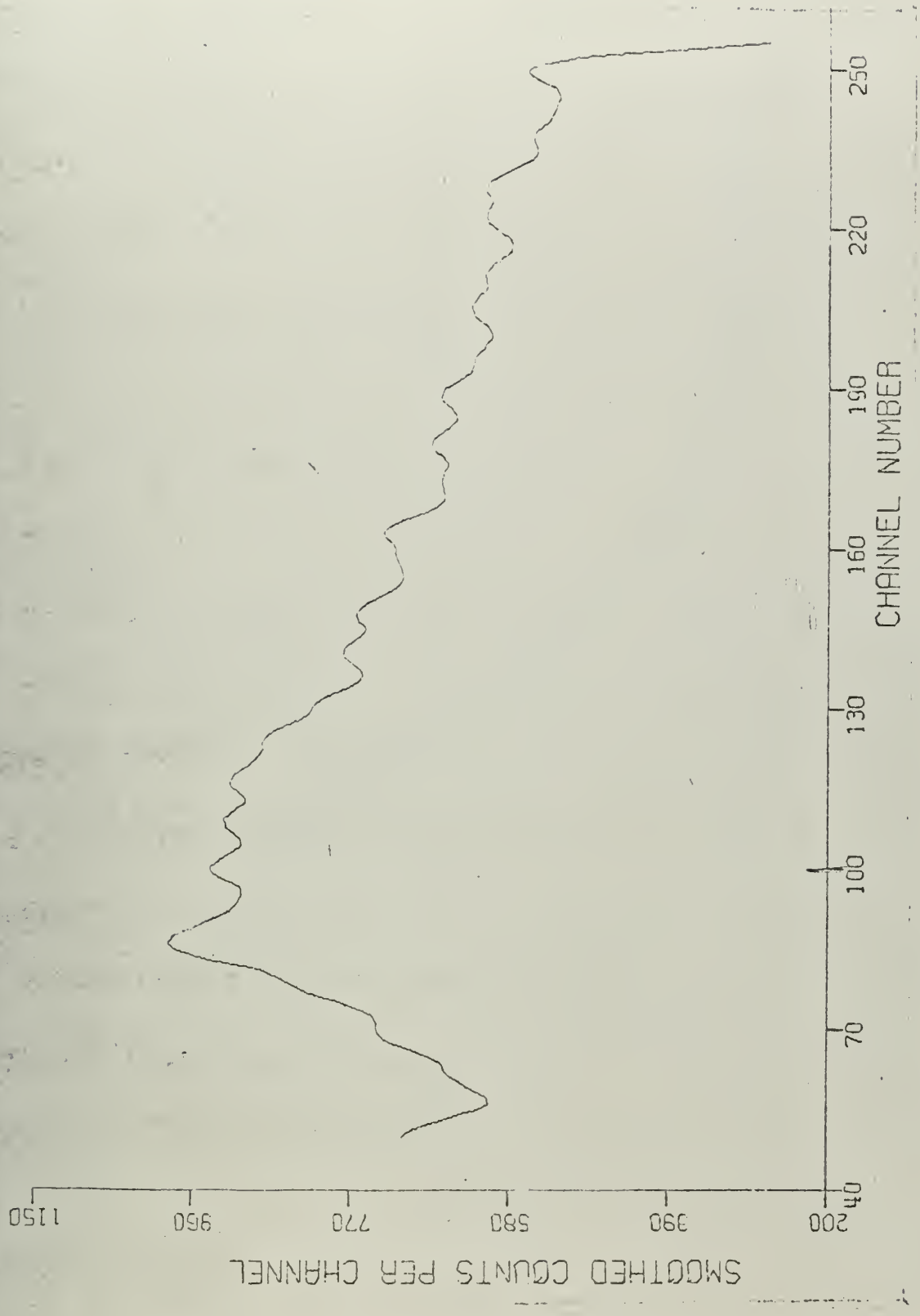

Figure 4.7 (b) Smoothed Version of Figure 4.7 (a)

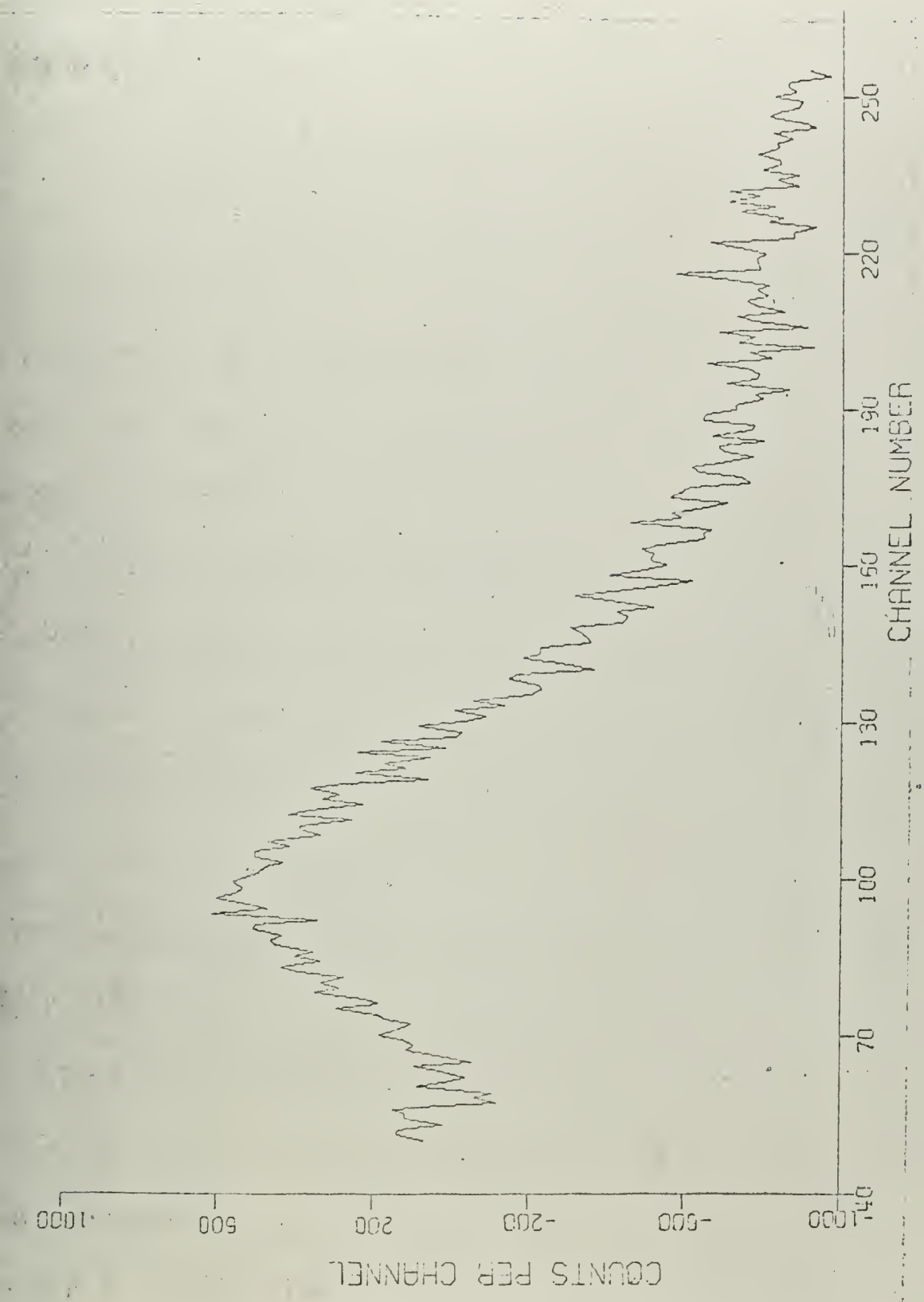

Figure 4.8 (a) Time Distribution at 1.46 eV and 18.0 cm Away From the Source

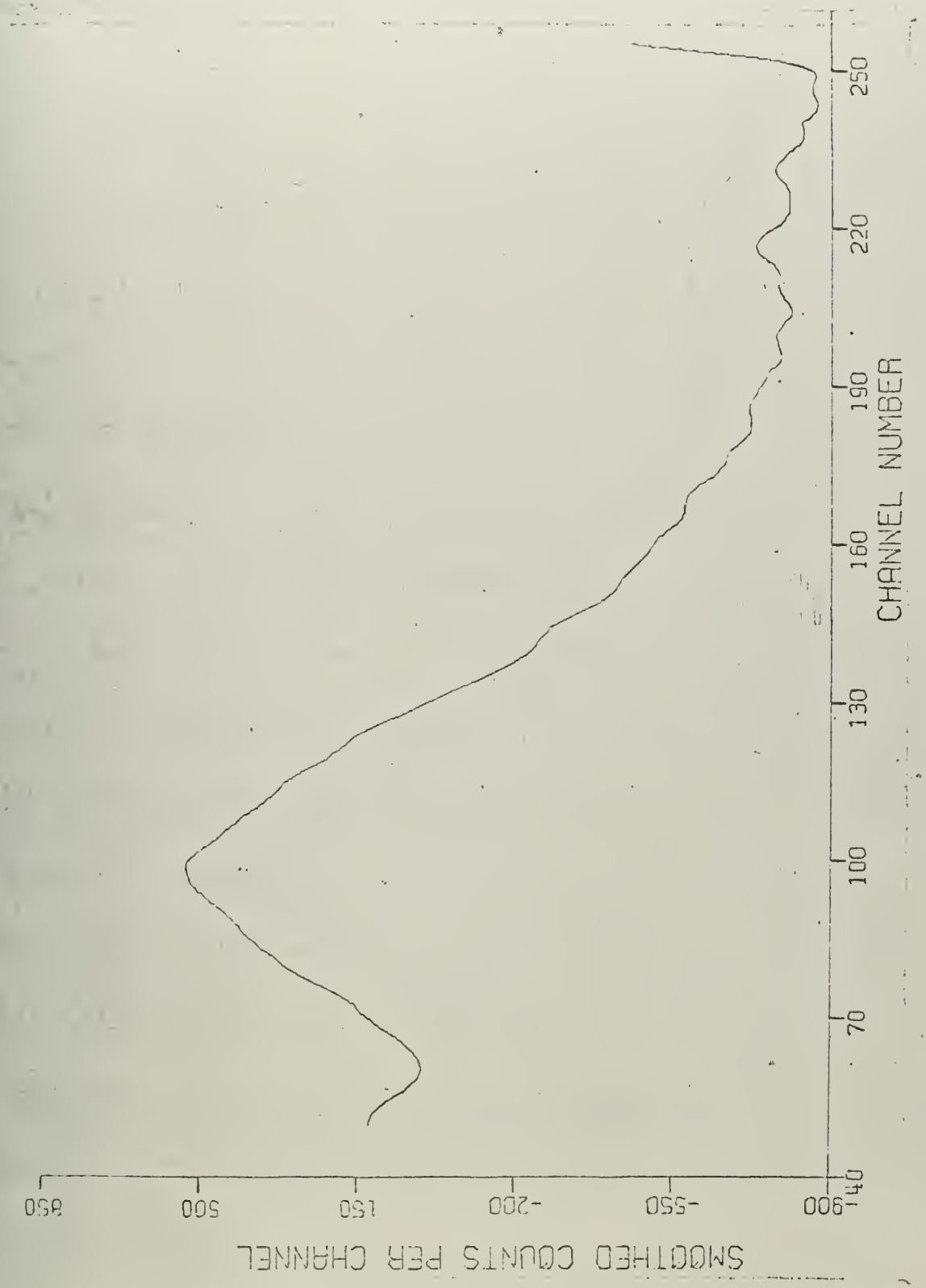

Figure 4.8 (b) Smoothed Version of Figure 4.8 (a)

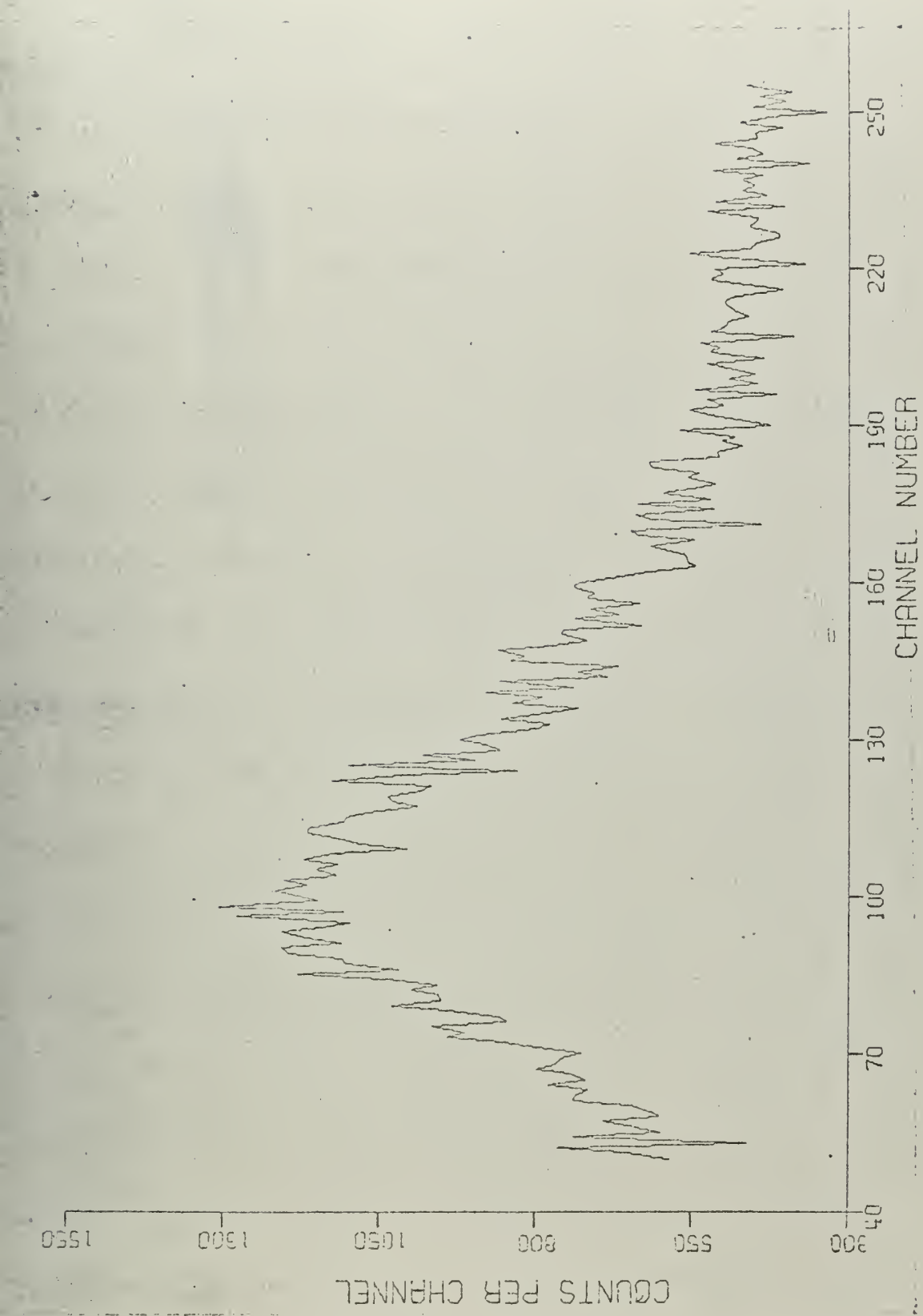

Figure 4.9 (a) Time Distribution at 1.46 eV and 28.0 cm Away From the Source

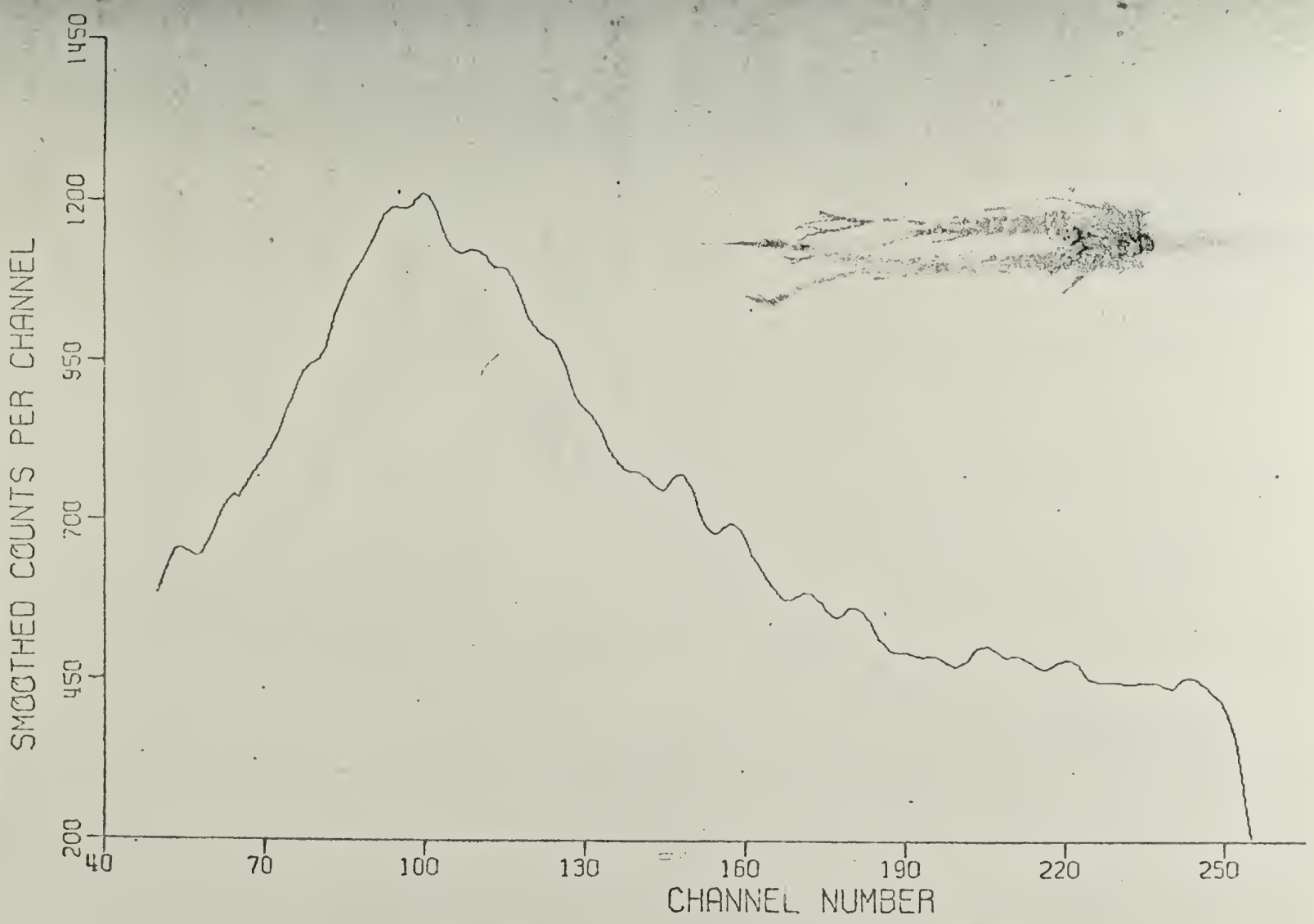

Figure 4.9 (b) Smoothed Version of Figure 4.9 (a)

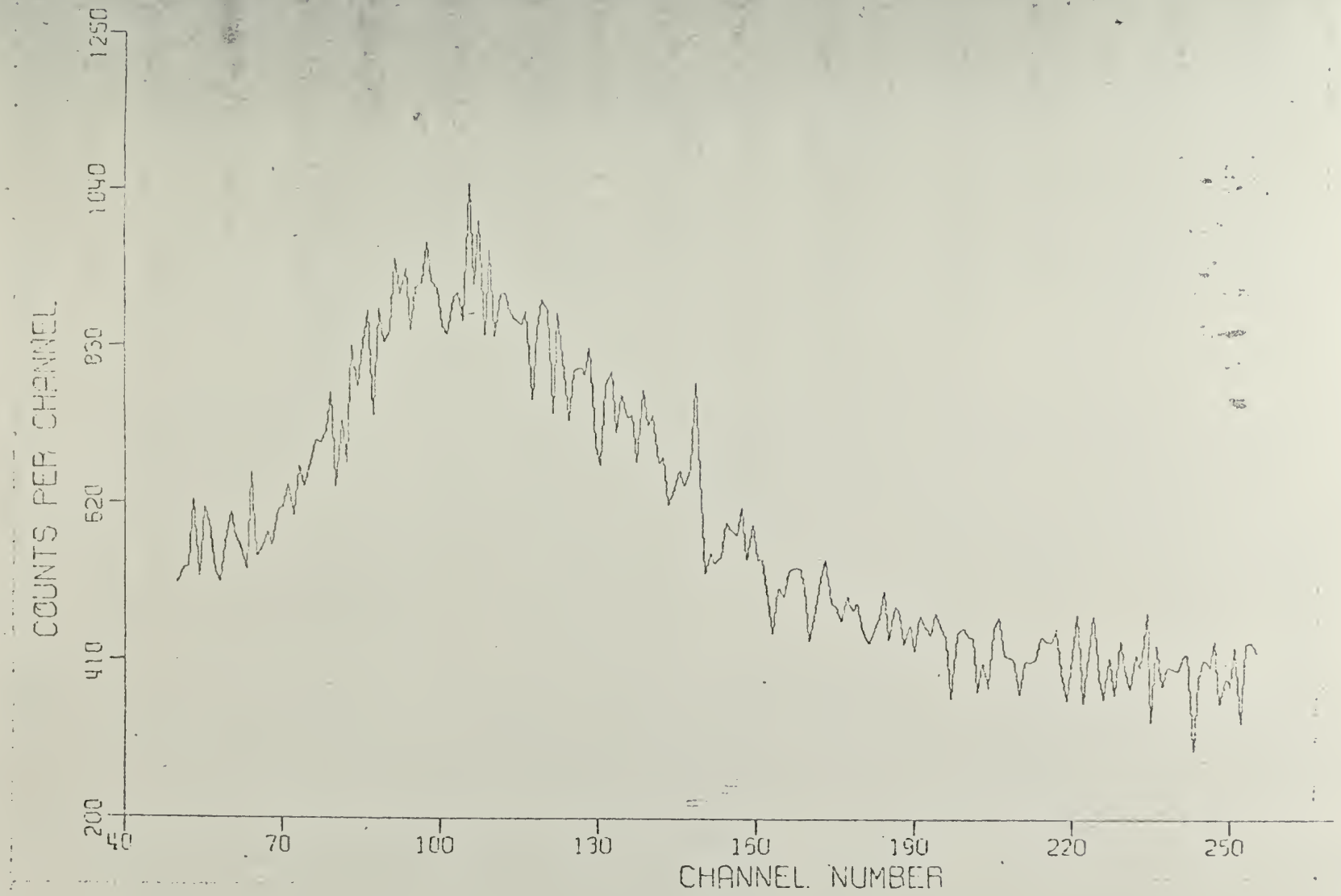

Figure 4.10 (a) Time Distribution at 1.46 eV and 37.5 cm Away From the Source

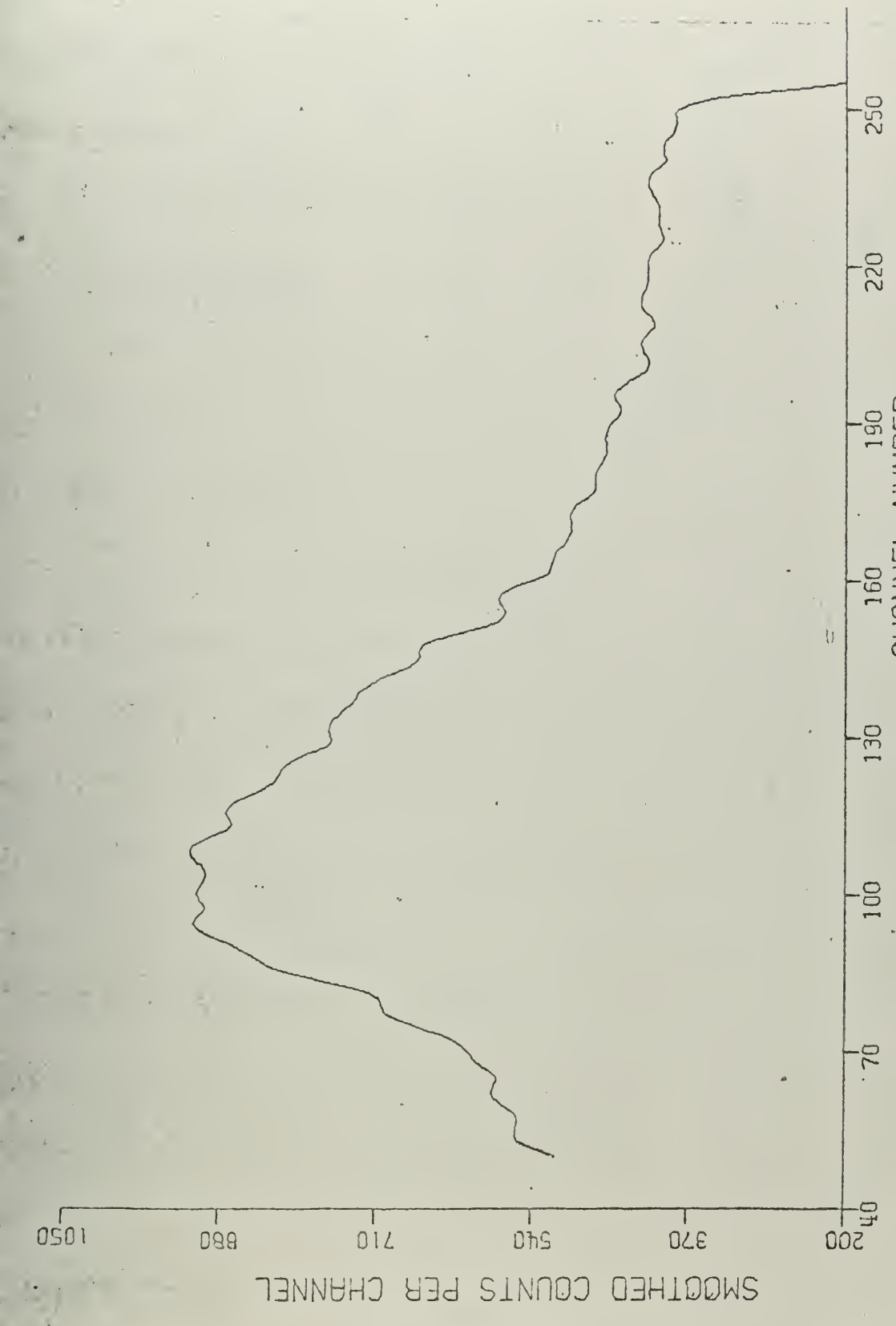

Figure 4.10 (b) Smoothed Version of Figure 4.10 (a)

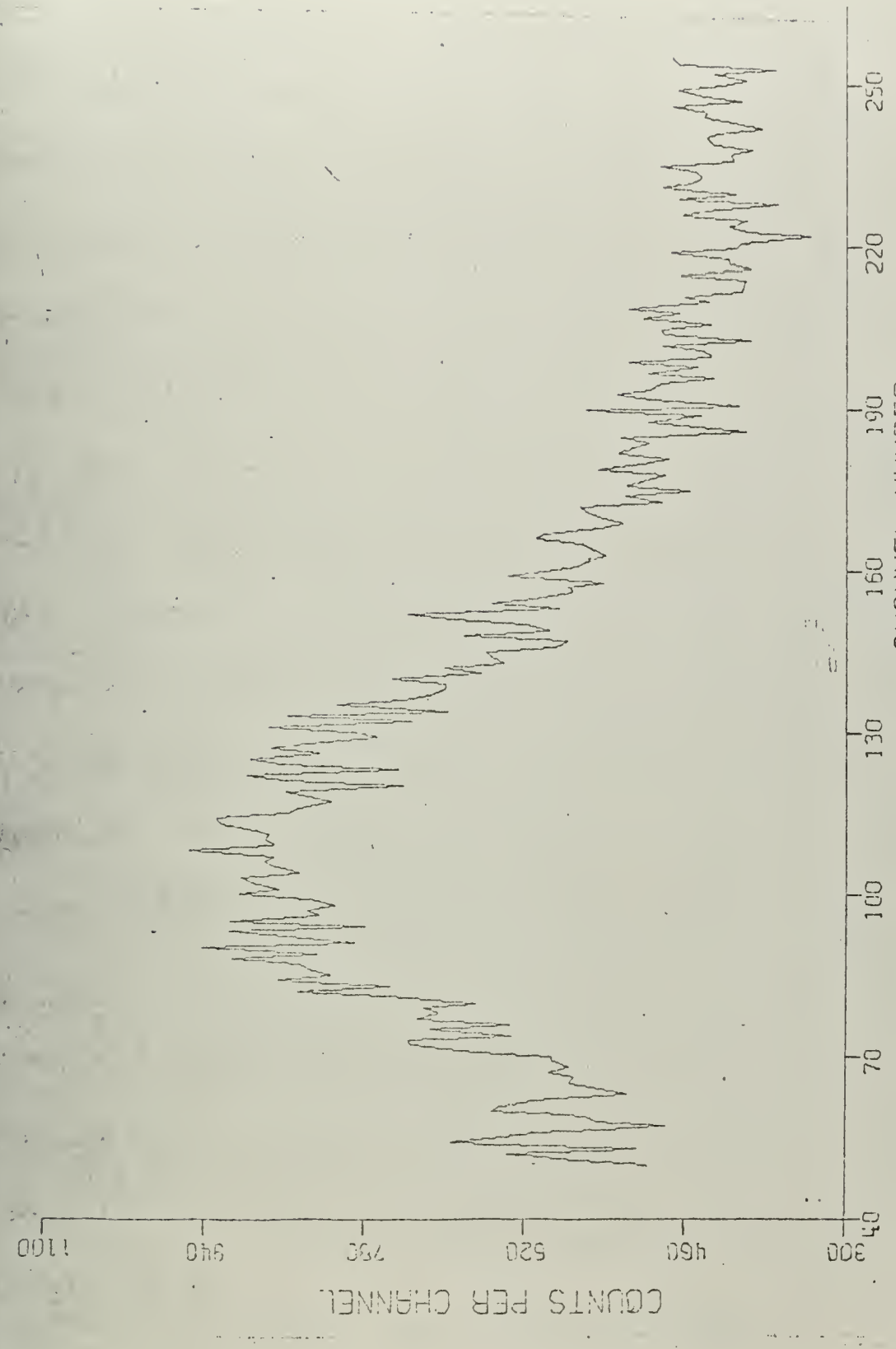

Figure 4.11 (a) Time Distribution at 1.46 eV and 44.5 cm Away From the Source

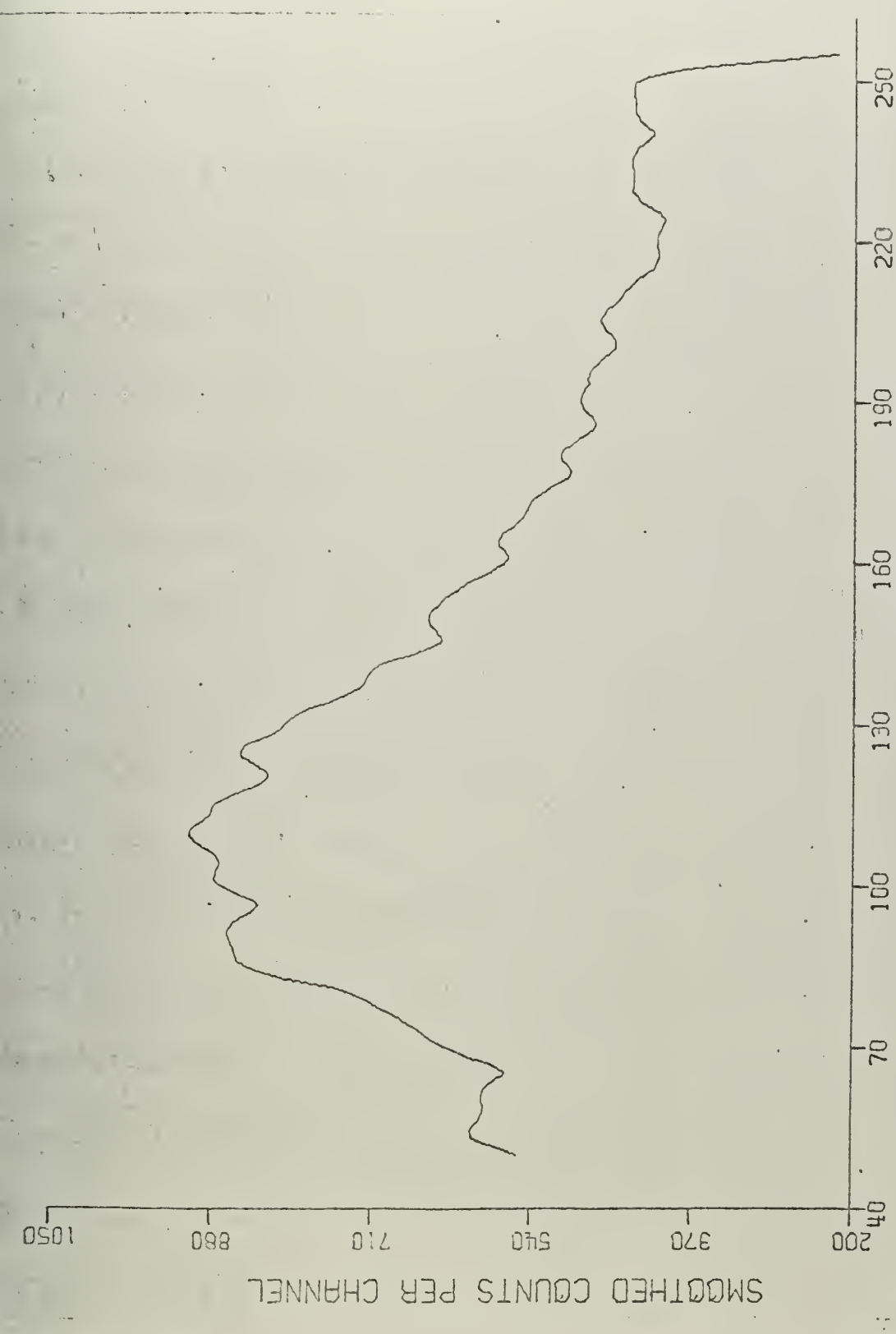

Figure 4.11 (b) Smoothed Version of Figure 4.11 (a)

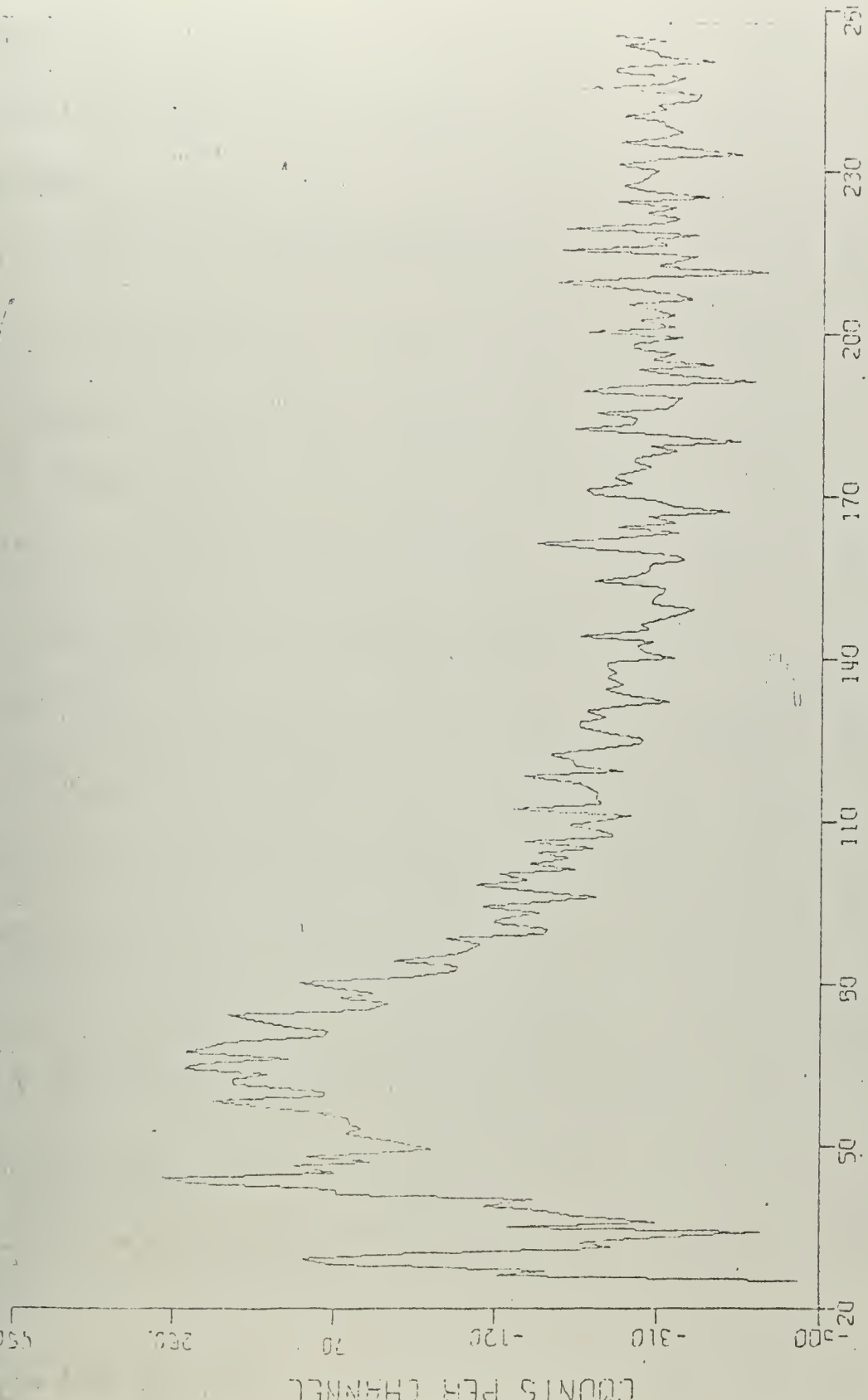

Figure 4.13 (a) Time Distribution at 5.0 eV and 12.5 cm Away From the Source

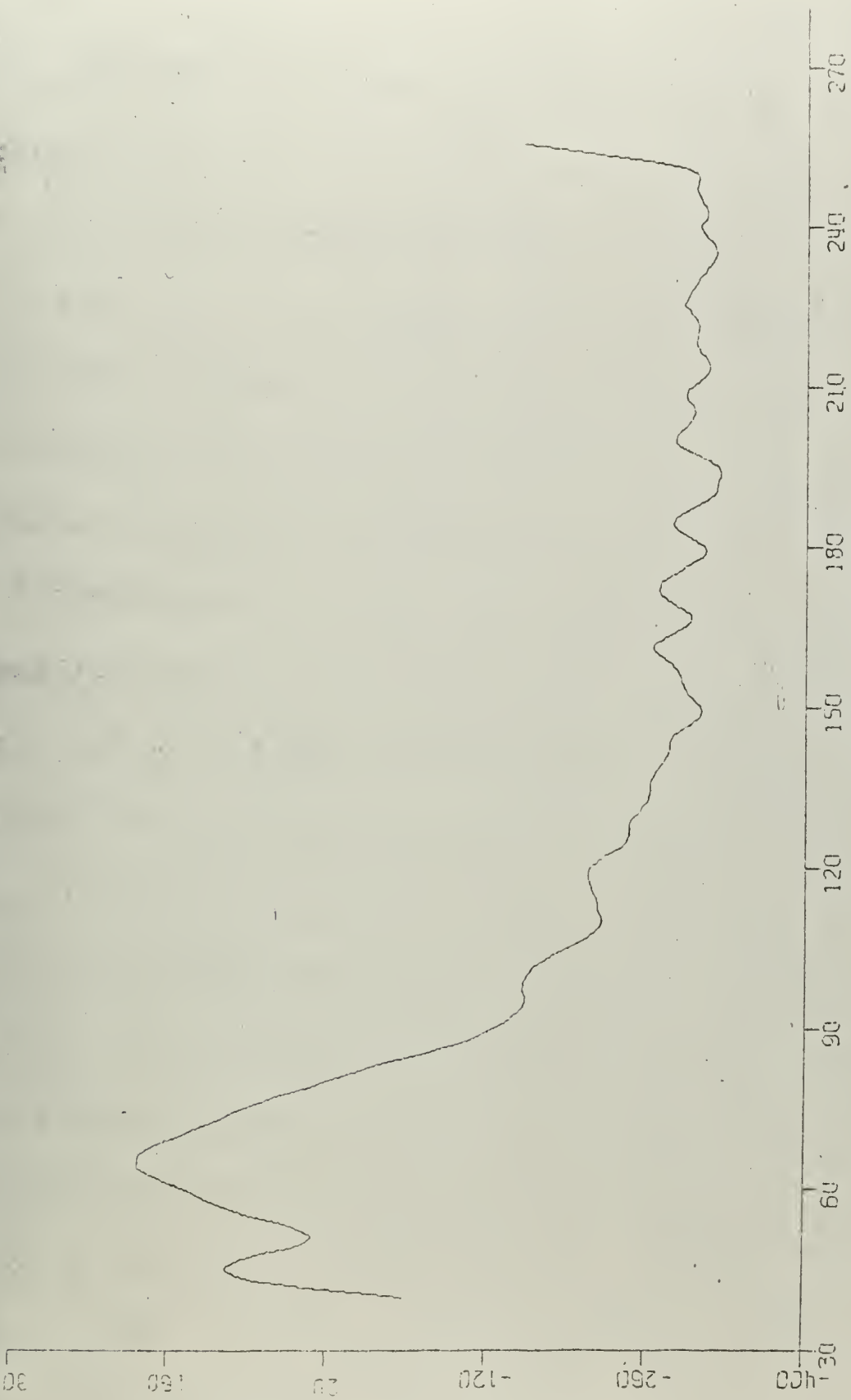

Figure 4.13 (b) Smoothed Version of Figure 4.13 (a)

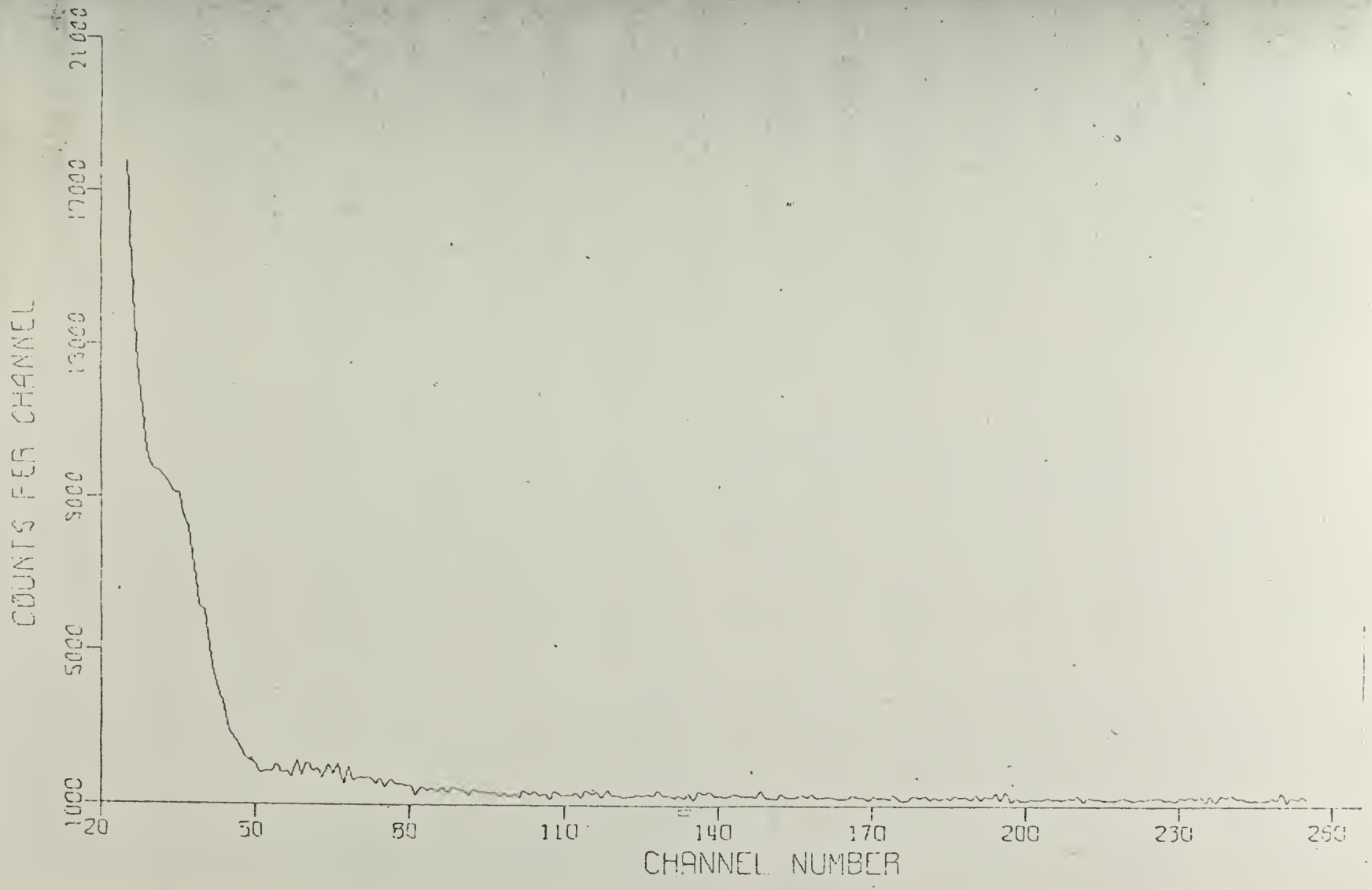

Figure 4.14 (a) Time Distribution at 5.0 eV and 18.0 cm Away From the Source

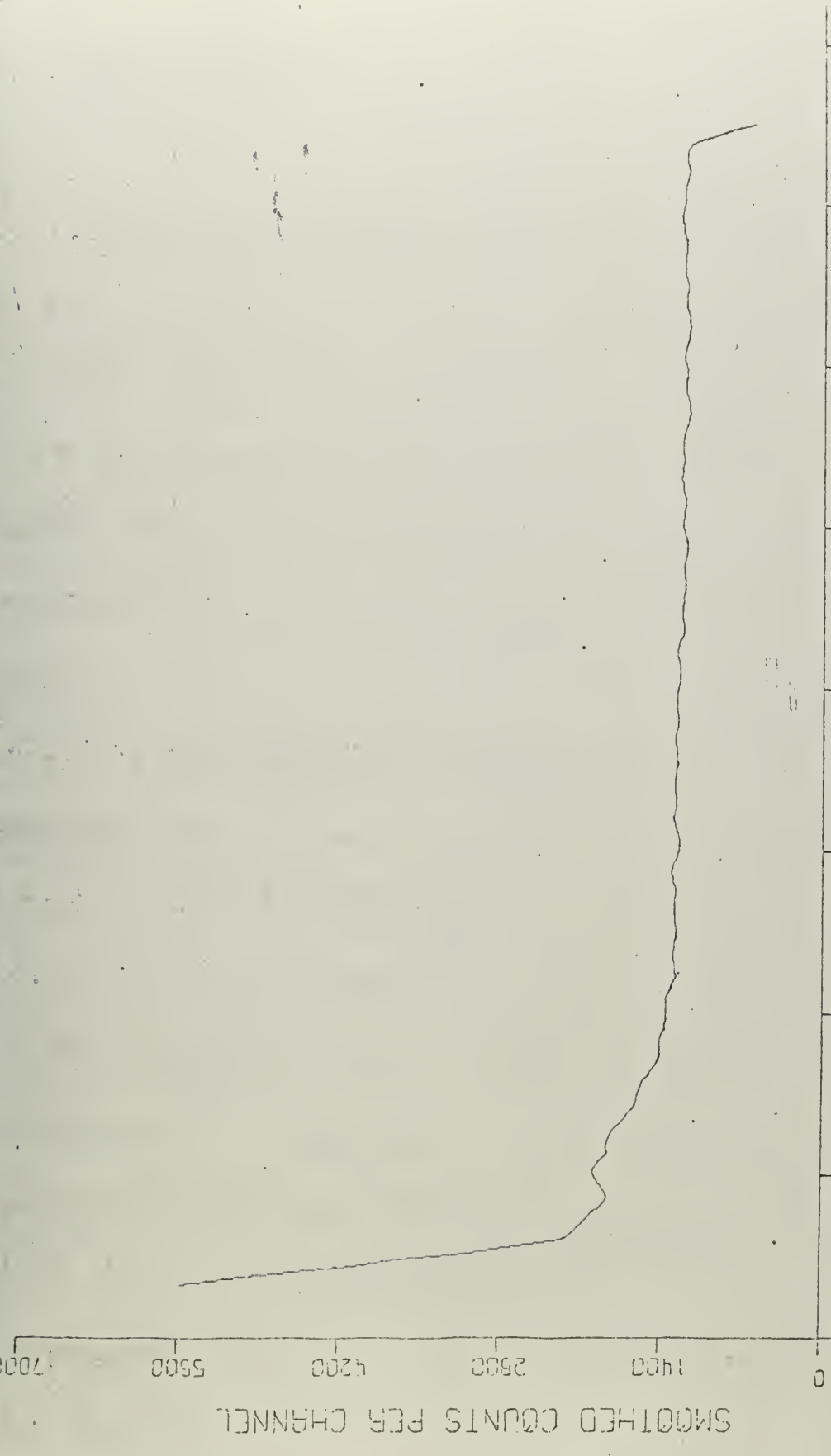

Figure 4.14 (b) Smoothed Version of Figure 4.14 (a)

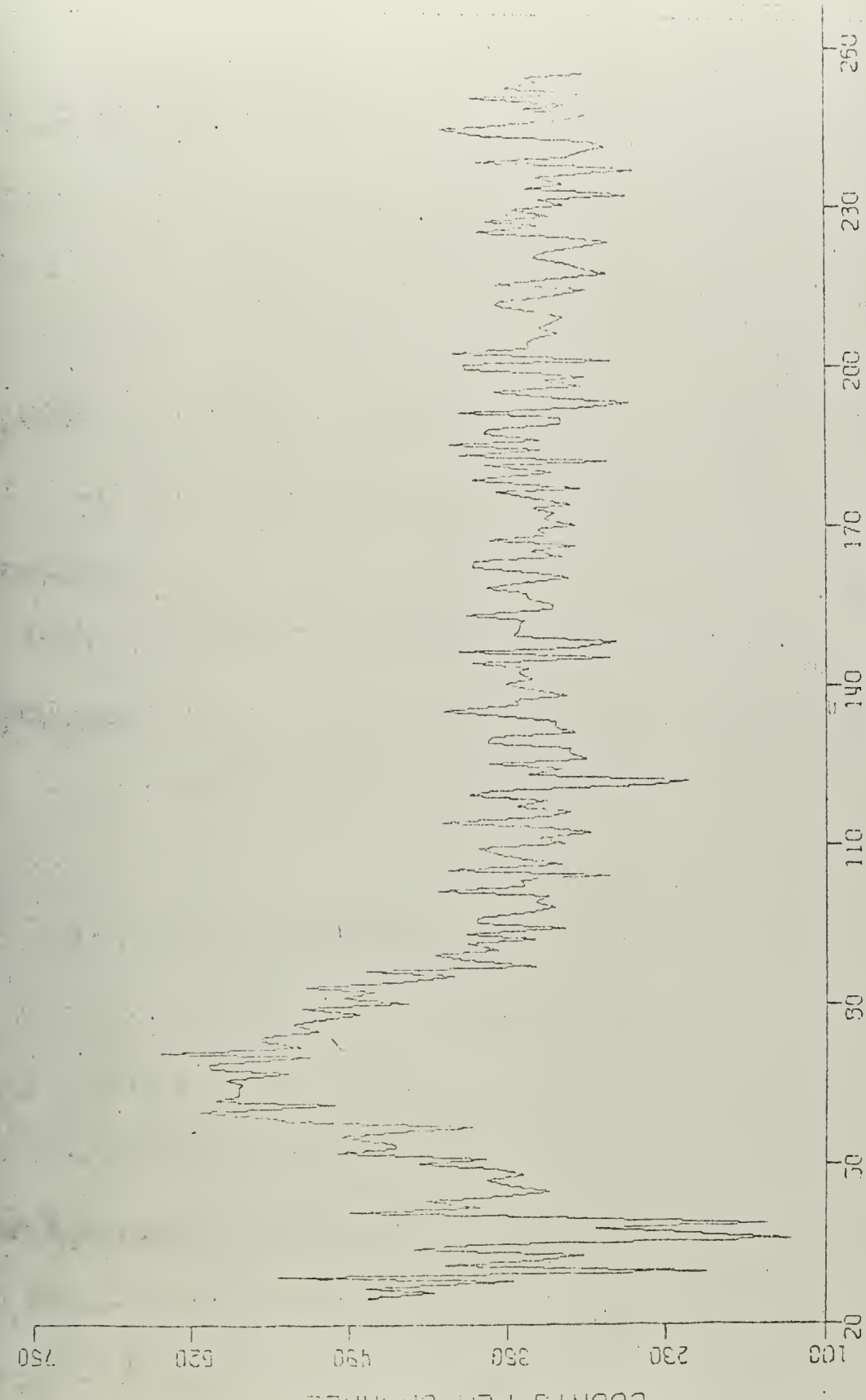

Figure 4.15 (a) Time Distribution at 5.0 eV and 37.5 cm Away From the Source

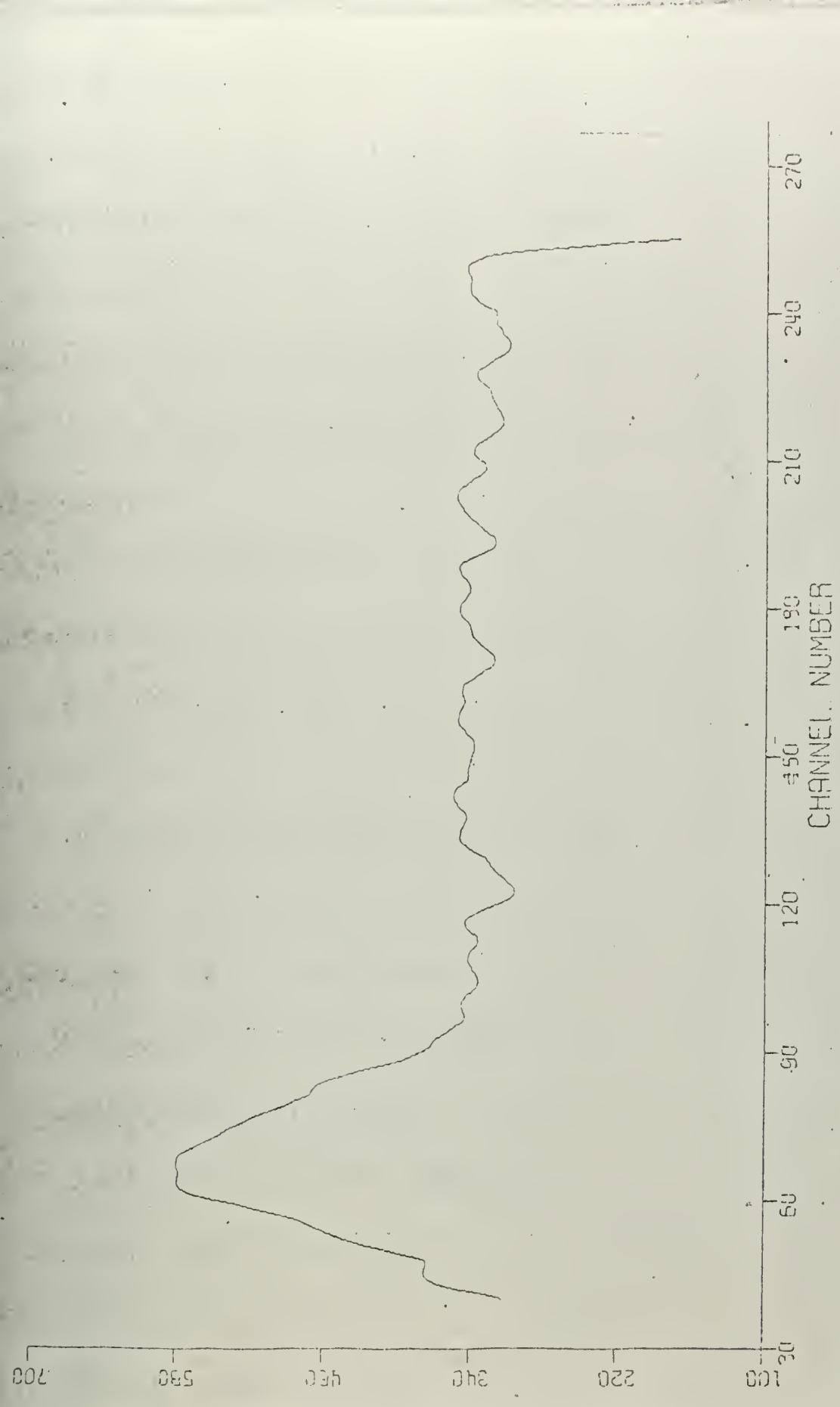

Figure 4.15 (b) - Smoothed Version of Figure 4.15 (a)

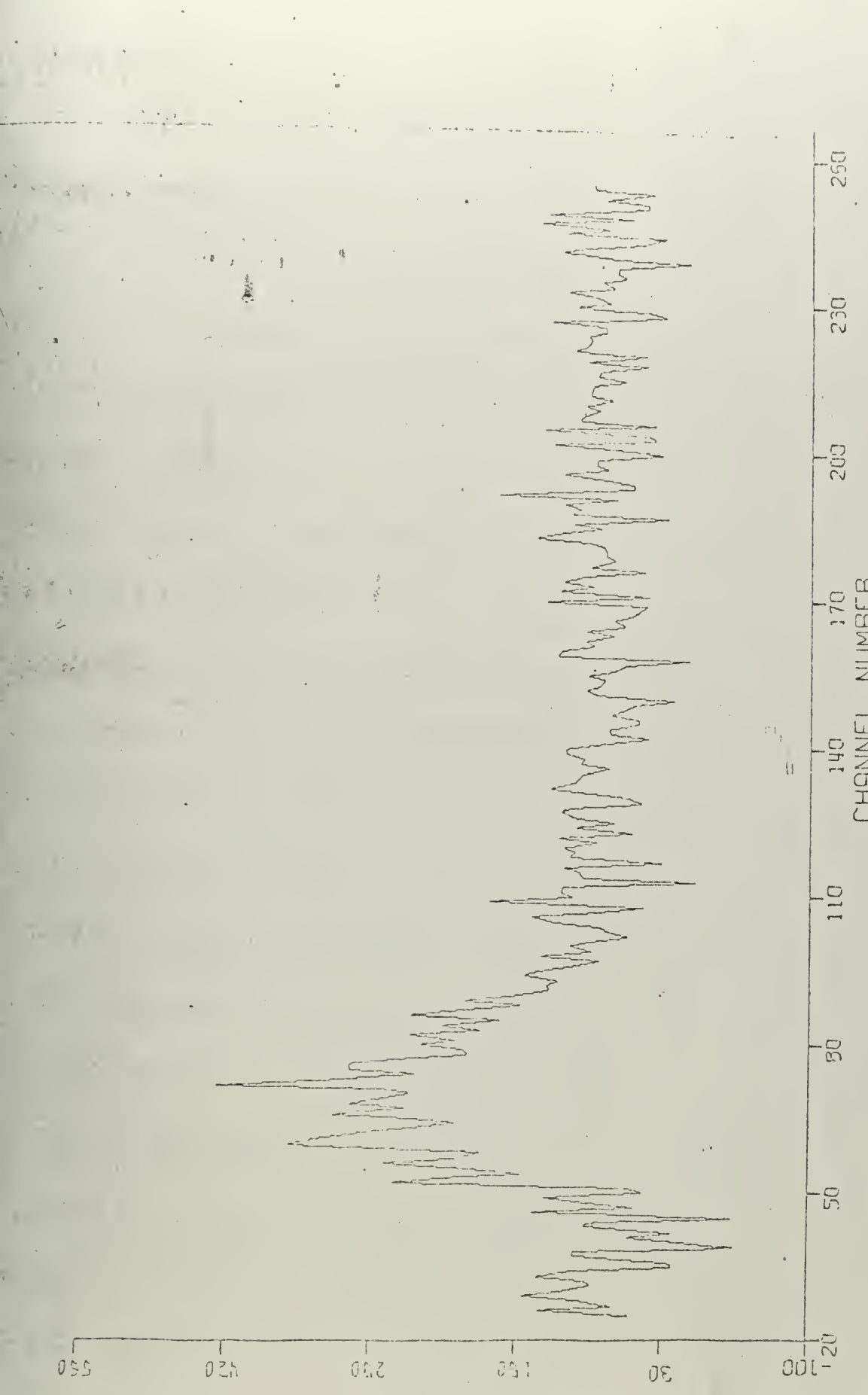

Figure 4.16 (a) Time Distribution at 5.0 eV and 44.0 cm Away From the Source

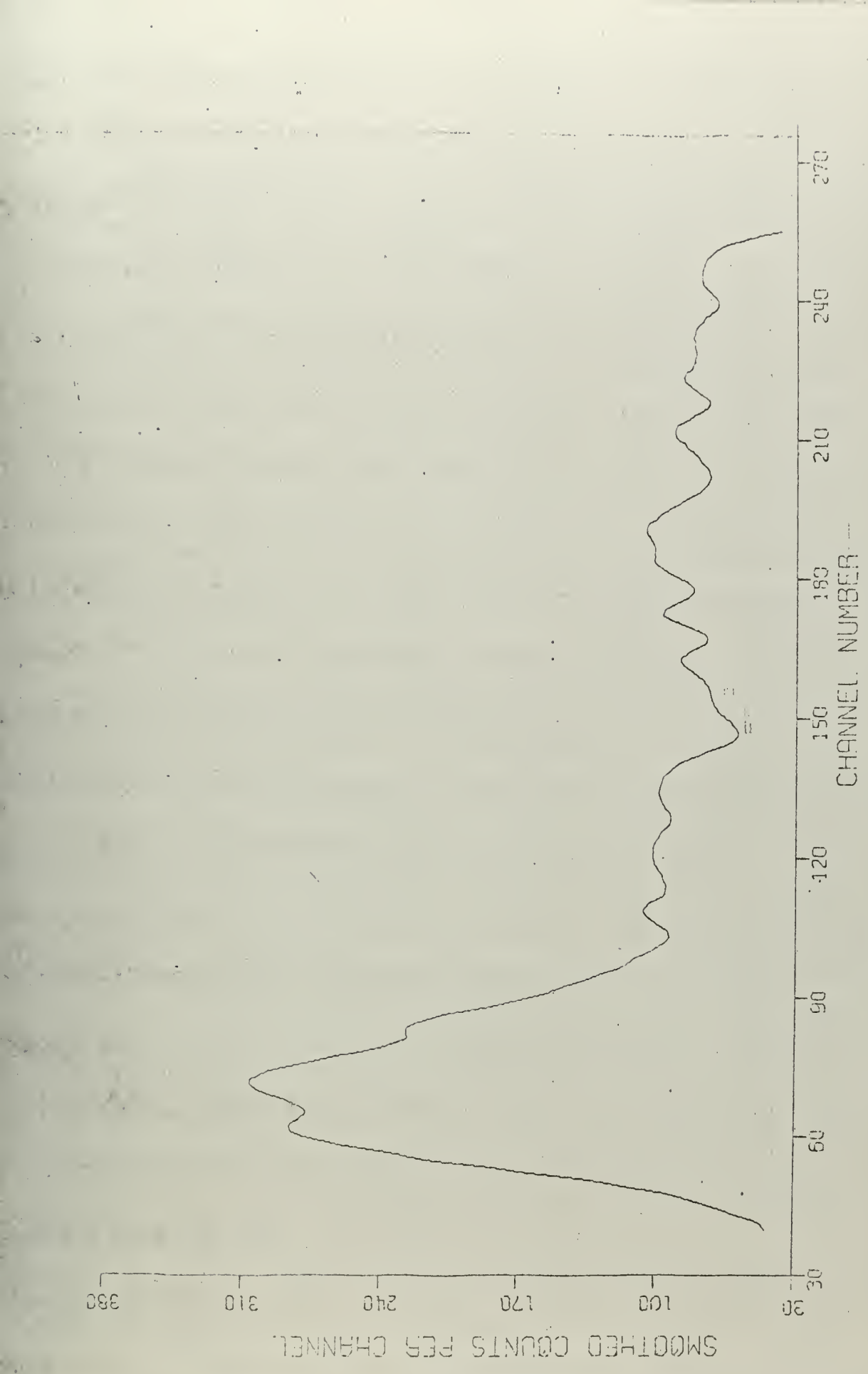

Figure 4.16 (b) Smoothed Version of Figure 4.16 (a)

t_m as shown by the experiments.

This disagreement between theory and experiment was probably due to the breakdown of the infinite medium boundary conditions, since the foil was only 9 cm from the outer edge of the assembly at the last spatial point. The absence of moderating material surrounding the foil meant that the neutrons took a longer time to slow down to a given energy. More measurements need to be taken at greater distances to resolve this question.

A few measurements were made with the detector separated from the foil by about 10 cm of graphite in order to determine if the perturbation caused by the detector had any effect on the slowing down time. These results are marked by triangles in the Figures. It can be seen that the gold and cadmium results agree, within the limits of experimental uncertaintity, with previous measurements. The indium point, however, falls far below the original measurements. The author can give no explanation for the contradiction of this point with either the original results for indium or the close agreement between the first and second measurements for the gold and cadmium. Further measurements, with the detector and foil separated, need to be performed to clear up this contradiction.

4.5 Conclusions

There was some agreement between the spatially dependent slowing down time measurements made in these experiments and theoretical calculations using diffusion theory.

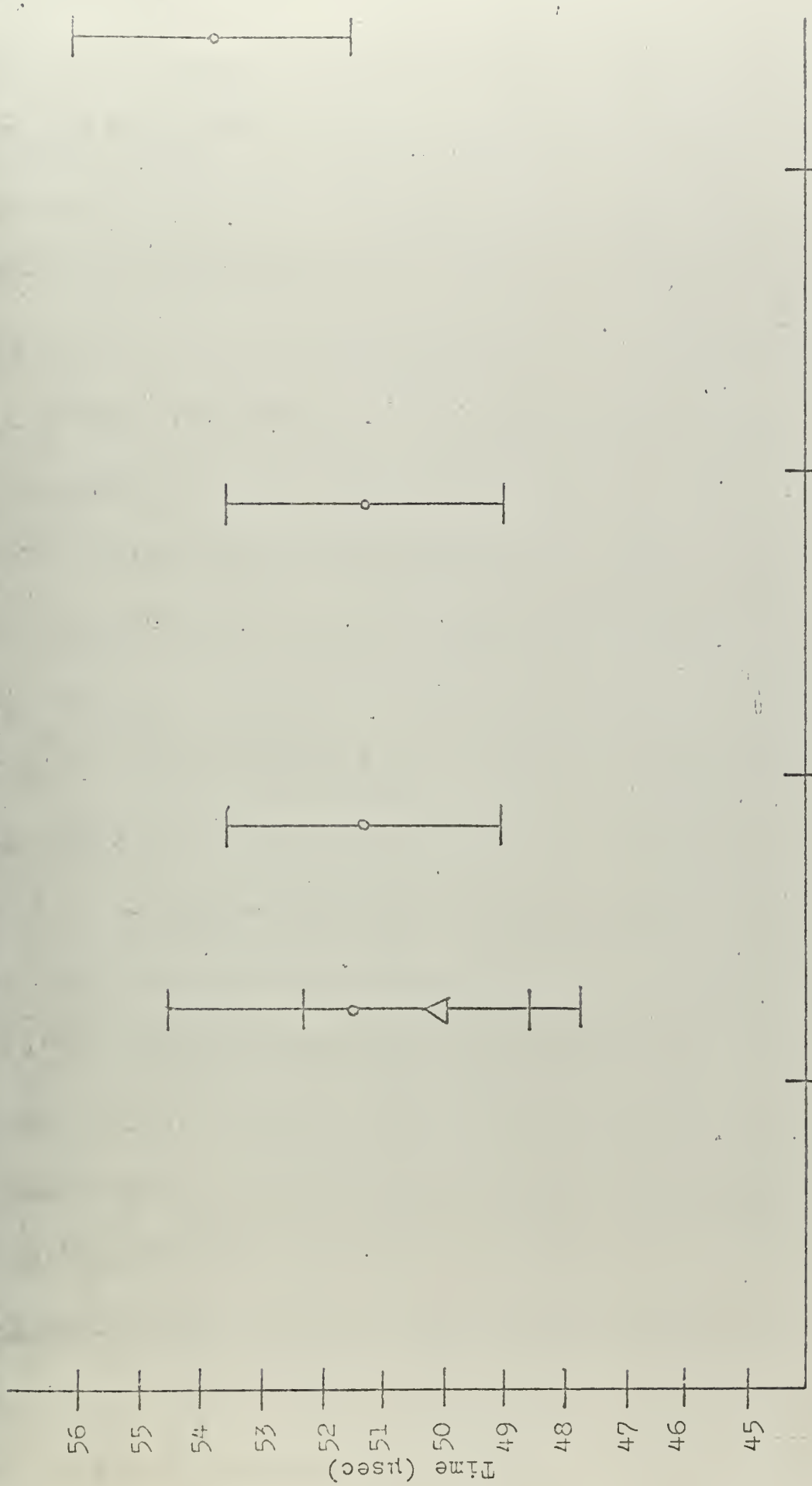

Figure 4.17 Slowing Down Time vs. Distance at 0.2 eV

Figure 4.18 Slowing Down Time vs. Distance at 1.46 eV

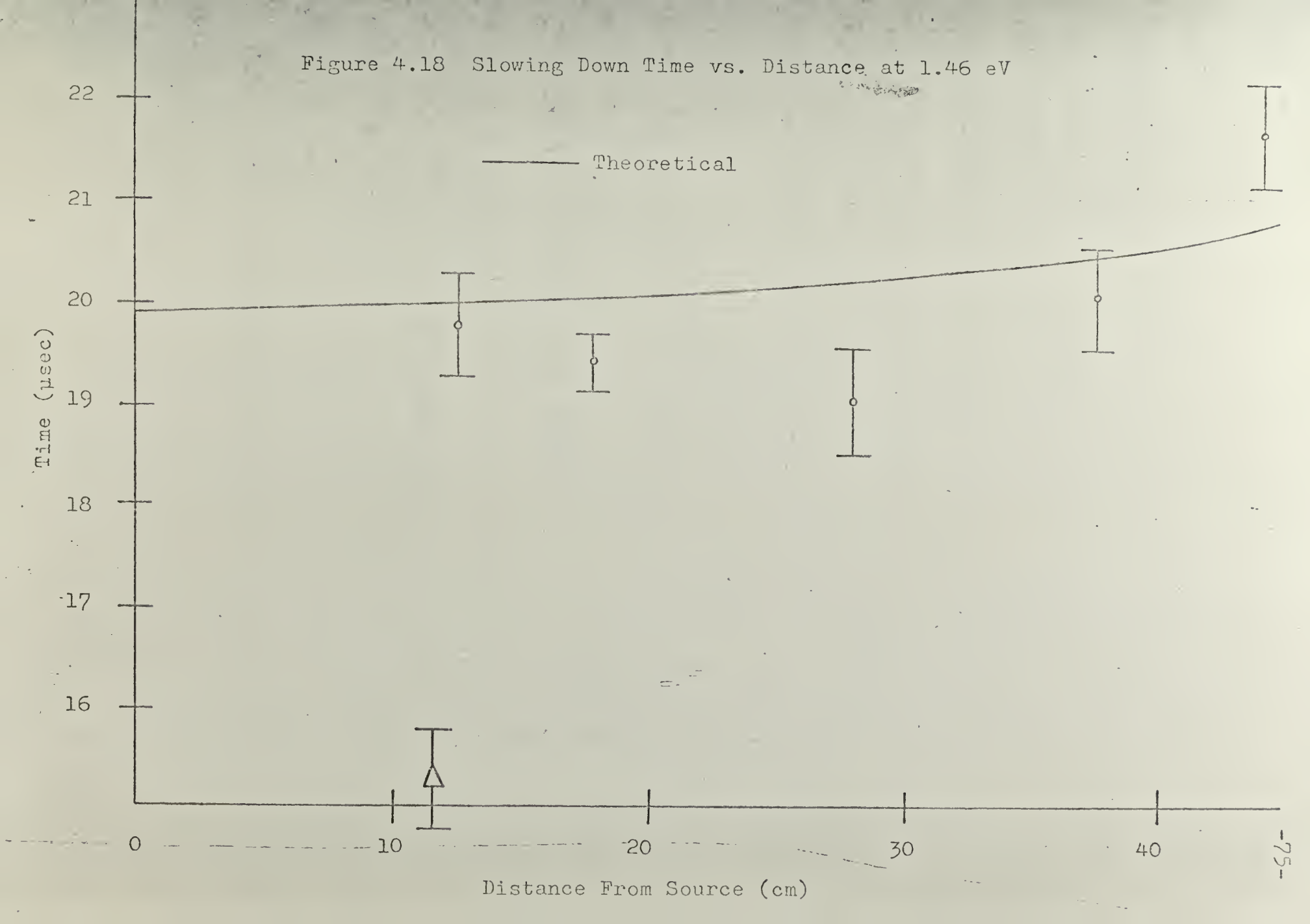

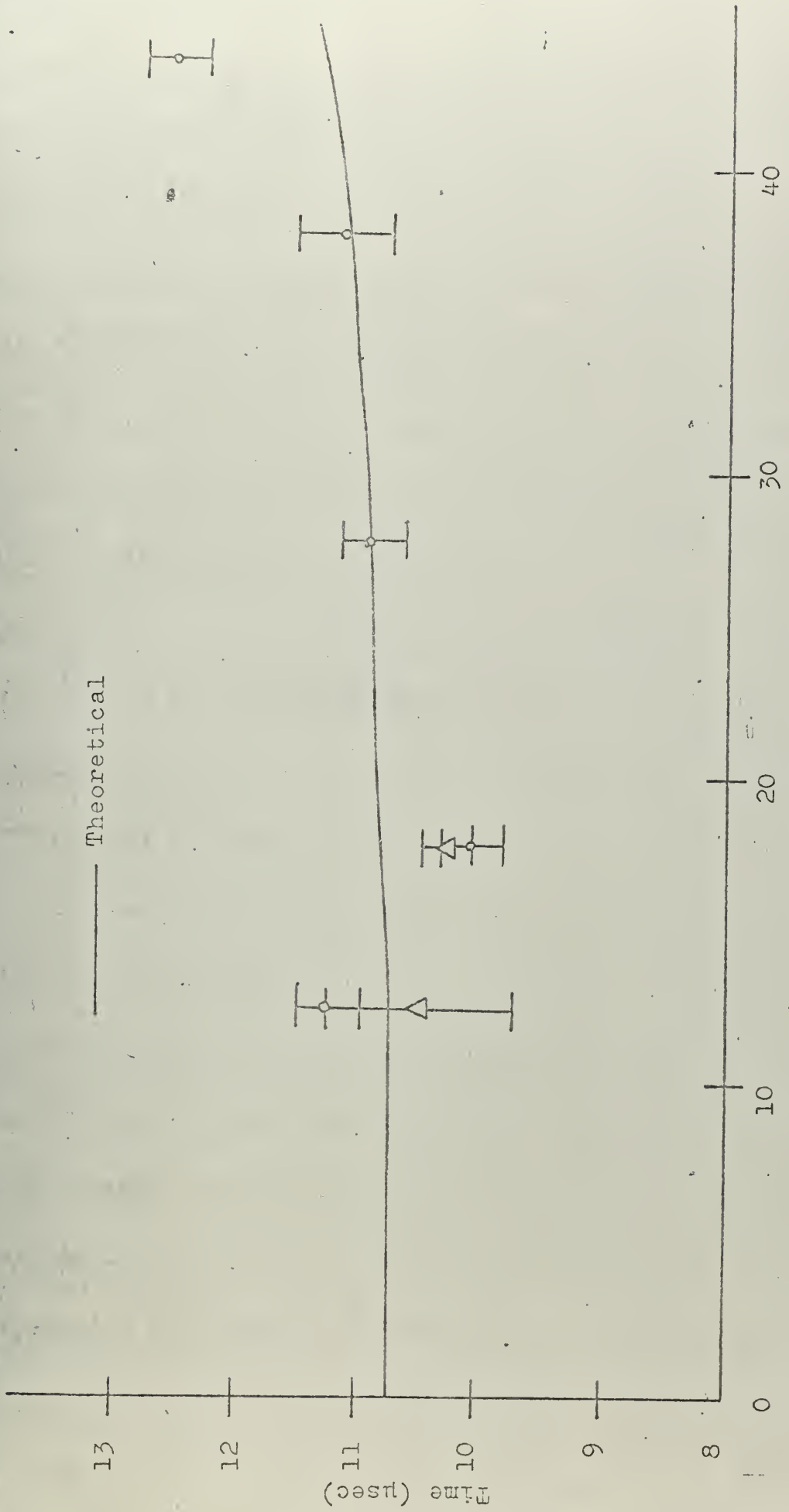

Figure 4.19 Slowing Down Time vs. Distance at 5.0 eV

No measurable spatial dependence of the slowing down time was observed for distances less than 30 cm. Spatial dependence was observed for distances greater than 30 cm, although this dependence was much more promounced in the experiments than predicted by slowing down theory. More space dependent measurements at distances greater than 44 cm should be made in a larger graphite assembly to determine the true spatial dependence. Measurements to determine if the perturbation of the detector had any effect on the slowing down time were inconclusive and should be repeated.

References for Chapter 4

1. A.G. Adamantiades, Ph.D. Thesis, Department of Nuclear Engineering M.I.T., (1966).

2. S.G. Oston, Ph.D. Thesis, Department of Nuclear Engineering M.I.T., (1966).

3. T. Inouye and N.C. Rasmussen, A Computer Method for the Analysis of Complex Gamma-Ray Spectra, Transactions of the American Nuclear Society, Illinois, 10 (1967).

4. D. Diamond, private correspondence, September (1966).

Appendix A. Computer Program Listings

A.1

```
C      NORMALIZATION, DEAD TIME CORRECTION, AND BACKGROUND
C      SUBTRACTION CODE LISTING
C
       DIMENSION TBM(255),CHAN(255),BACK(255),FOIL(255),ANORM(255),
      1CBACK(255),CFOIL(255),X(255),Y(255),TBA(206),ACHAN(206),B(800)
       COMMON TBM,CHAN,WIDTH
       EQUIVALENCE(TBM(50),TBA(1)),(CHAN(50),ACHAN(1))
       READ 200,WIDTH
   200 FORMAT(F6.2)
       READ 99,BCOUNT,FCOUNT
    99 FORMAT (2F10.0)
       NUM=0
   103 NUM=NUM+1
       READ 100,(BACK(I),I=1,255)
   100 FORMAT (3X,10F7.0)
       READ 101,(FOIL(I),I=1,255)
   101 FORMAT (3X,10F7.0)
       READ 98,BBUR,ABUR
    98 FORMAT (2F10.0)
       PRINT 701,BCOUNT,FCOUNT
   701 FORMAT (3X,2F10.0)
       PRINT 100,(BACK(I),I=1,255)
       PRINT 101,(FOIL(I),I=1,255)
       PRINT 702,BBUR,ABUR
   702 FORMAT (3X,2F10.0)
       L=-1
   420 L=L+1
       IF (L)419,419,417
   419 DO 418 I=1,255
   418 X(I)=BACK(I)
       BUR=BBUR
       GO TO 415
   417 DO 416 I=1,255
   416 X(I)=FOIL(I)
       BUR=ABUR
   415 DUM=16./WIDTH
       N=DUM
       Y(1)=BUR*LOGF(BUR/(BUR-X(1)))
       SUM=0.
       DO 610  I=2,N
       SUM=SUM+X(I-1)
```

```
  610 Y(I)=BUR*LOGF((BUR-SUM)/(BUR-SUM-X(I)))
      SUM=SUM+X(N)
        NM=N+1
      DO 615 I=NM,255
      Y(I)=BUR*LOGF((BUR-SUM)/(BUR-SUM-X(I)))
      K=I-N
  615 SUM=SUM+X(I)-X(K)
      IF (L)414,414,412
  414 DO 413 I=1,255
  413 CBACK(I)=Y(I)
       GO TO 420
  412 DO 411 I=1,255
  411 CFOIL(I)=Y(I)
      Z=BCOUNT/FCOUNT
      DO 906 I=1,255
      ANORM(I)=Z*CFOIL(I)
      TBM(I)=ANORM(I)-CBACK(I)
      CHAN(I)=FLOATF(I)
  906 CONTINUE
      PRINT 306,(TBM(I),I=1,255)
  306 FORMAT (1H ,10F10.1)
C
C     CALCOMP ROUTINES
C
   50 CALL PLOTS1(8,800)
      CALL SYMBL5(3.0,9.0,0.2,20H ID NO. = M3994-5788,0.,20)
      CALL NUMBR1(4.0,8.5,0.2,NUM,0.,-1)
      CALL PICTUR(8.5,4.2,15H CHANNEL NUMBER,
     115,19H COUNTS PER CHANNEL,19,ACHAN,TBA,206,0.,0)
      END FILE 10
C
      READ 99,BCOUNT,FCOUNT
      IF (BCOUNT)700,700,103
  700 CALL EXIT
      END
```

A.2

```
C      DATA SMOOTHING CODE LISTING INCLUDING NORMALIZATION, DEAD
C      TIME CORRECTION, AND BACKGROUND SUBTRACTION
C
       DIMENSION TBN(37),XSIN(75),SEIGEN(37,75),XCOS1(75),XCOS2(75),
      1XCOS4(37),TBM(255),TBK(255),CHAN(255),THETA(75),ALPHA(75),
      2BETA(75),GAMMA(75),WT(75),B(800),BACK(255),FOIL(255),ANORM(255),
      3CBACK(255),CFOIL(255),X(255),Y(255),TBA(216),ACHAN(216)
       COMMON TBN,XSIN,SEIGEN,XCOS1,XCOS2,XCOS4,TBM,TBK,CHAN,WIDTH
       EQUIVALENCE(TBK(40),TBA(1)),(CHAN(40),ACHAN(1))
       READ 200,IW,OMEGAH,CRT,FACTR,WIDTH
  200  FORMAT (I4,E10.4,F6.0,F6.3,F6.2)
       READ 102,(WT(I),I=1,IW)
  102  FORMAT (12F6.3)
       PRINT 201,IW,OMEGAH,CRT,FACTR,WIDTH
  201  FORMAT (1H1,9H N-OMEGA=,I4,1X,9H D-OMEGA=,E10.4,1X,
      15H CRT=,F6.0,1X,8H FACTOR=,F6.3,7H WIDTH=,F6.2)
       PRINT 205
  205  FORMAT (1H ,20X,16H WEIGHT FUNCTION)
       PRINT 203,(WT(I),I=1,IW)
  203  FORMAT (1H ,5E15.7)
       READ 99,BCOUNT,FCOUNT
   99  FORMAT (2F10.0)
       NUM=0
  103  NUM=NUM+1
       READ 100,(BACK(I),I=1,255)
  100  FORMAT (3X,10F7.0)
       READ 101,(FOIL(I),I=1,255)
  101  FORMAT (3X,10F7.0)
       READ 98,BBUR,ABUR
   98  FORMAT (2F10.0)
       PRINT 701,BCOUNT,FCOUNT
  701  FORMAT (3X,2F10.0)
       PRINT 100,(BACK(I),I=1,255)
       PRINT 101,(FOIL(I),I=1,255)
       PRINT 702,BBUR,ABUR
  702  FORMAT (3X,2F10.0)
       L=-1
  420  L=L+1
       IF (L)419,419,417
  419  DO 418 I=1,255
  418  X(I)=BACK(I)
       BUR=BBUR
       GO TO 415
  417  DO 416 I=1,255
  416  X(I)=FOIL(I)
       BUR=ABUR
```

```
415 DUM=16./WIDTH
    N=DUM
    Y(I)=BUR*LOGF(BUR/(BUR-X(1)))
    SUM=0.
    DO 610  I=2,N
    SUM=SUM+X(I-1)
610 Y(I)=BUR*LOGF((BUR-SUM)/(BUR-SUM-X(I)))
    SUM=SUM+X(N)
      NM=N+1
    DO 615 I=NM,255
    Y(I)=BUR*LOGF((BUR-SUM)/(BUR-SUM-X(I)))
    K=I-N
615 SUM=SUM+X(I)-X(K)
    IF (L)414,414,412
414 DO 413 I=1,255
413 CBACK(I)=Y(I)
     GO TO 420
412 DO 411 I=1,255
411 CFOIL(I)=Y(I)
    DO 905 I=1,37
    YKAKU4=OMEGAH*FLOATF(IW-1)*FLOATF(I)
    XCOS4(I)=COSF(YKAKU4)
905  CONTINUE
    DO 901 I=1,37
    DO 902 J=1,IW
    XKAKU=OMEGAH*FLOATF(I)*FLOATF(J-1)
    SEIGEN(I,J)=SINF(XKAKU)
902  CONTINUE
901  CONTINUE
    DO 903 J=1,IW
    THETA(J)=OMEGAH*FLOATF(J-1)
    ALPHA(J)=THETA(J)**(-3)*(THETA(J)**2+THETA(J)*SEIGEN(1,J)*
   1COSF(THETA(J))-2.*SEIGEN(1,J)**2)
    BETA(J)=2.*THETA(J)**(-3)*(THETA(J)*(1.+COSF(THETA(J))**2)-2.*
   1SEIGEN(1,J)*COSF(THETA(J)))
    GAMMA(J)=4.*THETA(J)**(-3)*(SEIGEN(1,J)-THETA(J)*COSF(THETA(J)))
903  CONTINUE
    DO 906 I=1,255
    Z=BCOUNT/FCOUNT
    ANORM(I)=Z*CFOIL(I)
    IBM(I)=ANORM(I)-CBACK(I)
906 CONTINUE
    DO 15 I=1,27
```

```
      DO 904 J=1,IW
      YKAKU1=OMEGAH*FLOATF(J-1)
      YKAKU2=27.*YKAKU1
      XCOS1(J)=COSF(YKAKU1)
      XCOS2(J)=COSF(YKAKU2)
  904 CONTINUE
      DO 511 I=1,IW
      YA=ALPHA(I)
      YB=BETA(I)
      YC=GAMMA(I)
      SIG4=0.
      SIG3=0.5*(TBN(1)*SEIGEN(1,I)+TBN(27)*SEIGEN(27,I))
      DO 1 NN=3,25,2
    1 SIG3=SIG3+TBN(NN)*SEIGEN(NN,I)
      DO 2 NN=2,26,2
    2 SIG4=SIG4+TBN(NN)*SEIGEN(NN,I)
      XA=YA*(TBN(1)*XCOS1(I)-TBN(27)*XCOS2(I))+YB*SIG3+YC*SIG4
      XSIN(I)=XA*WT(I)
  511 CONTINUE
      DO 517 IX=1,16
      YA=ALPHA(IX+1)
      YB=BETA(IX+1)
      YC=GAMMA(IX+1)
      SIG4=0.
      SIG3=0.5*(XSIN(1)*SEIGEN(IX,1)+XSIN(IW)*SEIGEN(IX,IW))
      NY=IW-2
      DO 3 NN=3,NY,2
    3 SIG3=SIG3+XSIN(NN)*SEIGEN(IX,NN)
      NY=IW-1
      DO 4 NN=2,NY,2
    4 SIG4=SIG4+XSIN(NN)*SEIGEN(IX,NN)
      XA=OMEGAH*(YA*(XSIN(1)-XSIN(IW)*XCOS4(IX))+YB*SIG3+YC*SIG4)
      IN=IX
      TBK(IN)=0.63662*XA
      CHAN(IN)=FLOATF(IN)
  517 CONTINUE
      DO 914 J=1,IW
      YKAKU1=OMEGAH*FLOATF(J-1)
      YKAKU2=37.*YKAKU1
      XCOS1(J)=COSF(YKAKU1)
      XCOS2(J)=COSF(YKAKU2)
```

```
914   CONTINUE
      DO 530 J=2,15
      DO 525 I=1,37
      K=16*(J-1)-10+I
525   TBN(I)=TBM(K)
      DO 521 I=1,IW
      YA=ALPHA(I)
      YB=BETA(I)
      YC=GAMMA(I)
      SIG4=0.
      SIG3=0.5*(TBN(1)*SEIGEN(1,I)+TBN(37)*SEIGEN(37,I))
      DO 5 NN=3,35,2
    5 SIG3=SIG3+TBN(NN)*SEIGEN(NN,I)
      DO 6 NN=2,36,2
    6 SIG4=SIG4+TBN(NN)*SEIGEN(NN,I)
      XA=YA*(TBN(1)*XCOS1(I)-TBN(37)*XCOS2(I))+YB*SIG3+YC*SIG4
      XSIN(I)=XA*WT(I)
521   CONTINUE
      DO 527 IX=11,26
      YA=ALPHA(IX+1)
      YB=BETA(IX+1)
      YC=GAMMA(IX+1)
      SIG4=0.
      SIG3=0.5*(XSIN(1)*SEIGEN(IX,1)+XSIN(IW)*SEIGEN(IX,IW))
      NY=IW-2
      DO 7 NN=3,NY,2
    7 SIG3=SIG3+XSIN(NN)*SEIGEN(IX,NN)
      NY=IW-1
      DO 8 NN=2,NY,2
    8 SIG4=SIG4+XSIN(NN)*SEIGEN(IX,NN)
      XA=OMEGAH*(YA*(XSIN(1)-XSIN(IW)*XCOS4(IX))+YB*SIG3+YC*SIG4)
      IN=16*(J-1)+IX-10
      TBK(IN)=0.63662*XA
      CHAN(IN)=FLOATF(IN)
527   CONTINUE
530   CONTINUE
      DO 535 I=1,25
      K=230+I
535   TBN(I)=TBM(K)
      DO 924 J=1,IW
      YKAKU1=OMEGAH*FLOATF(J-1)
      YKAKU2=25.*YKAKU1
      XCOS1(J)=COSF(YKAKU1)
      XCOS2(J)=COSF(YKAKU2)
```

```
  924  CONTINUE
       DO 531 I=1,IW
       YA=ALPHA(I)
       YB=BETA(I)
       YC=GAMMA(I)
       SIG4=0.
       SIG3=0.5*(TBN(1)*SEIGEN(1,I)+TBN(25)*SEIGEN(25,I))
       DO 9 NN=3,23,2
    9  SIG3=SIG3+TBN(NN)*SEIGEN(NN,I)
       DO 10 NN=2,24,2
   10  SIG4=SIG4+TBN(NN)*SEIGEN(NN,I)
       XA=YA*(TBN(1)*XCOS1(I)-TBN(25)*XCOS2(I))+YB*SIG3+YC*SIG4
       XSIN(I)=XA*WT(I)
  531  CONTINUE
       DO 537 IX=11,25
       YA=ALPHA(IX+1)
       YB=BETA(IX+1)
       YC=GAMMA(IX+1)
       SIG4=0.
       SIG3=0.5*(XSIN(1)*SEIGEN(IX,1)+XSIN(IW)*SEIGEN(IX,IW))
       NY=IW-2
       DO 11 NN=3,NY,2
   11  SIG3=SIG3+XSIN(NN)*SEIGEN(IX,NN)
       NY=IW-1
       DO 12 NN=2,NY,2
   12  SIG4=SIG4+XSIN(NN)*SEIGEN(IX,NN)
       XA=OMEGAH*(YA*(XSIN(1)-XSIN(IW)*XCOS4(IX))+YB*SIG3+YC*SIG4)
       IN=230+IX
       TBK(IN)=0.63662*XA
       CHAN(IN)=FLOATF(IN)
  537  CONTINUE
       PRINT 307
  307  FORMAT (1H1,18H SMOOTHED FUNCTION)
       PRINT 306,(TBK(I),I=1,255)
  306  FORMAT (1H ,10F10.1)
C
C      CALCOMP ROUTINES
C
   50  CALL PLOTS1(B,800)
       CALL NUMBR1(4.0,8.5,0.2,NUM,0.,-1)
       CALL SYMBL5(3.0,9.0,0.2,20H ID NO. = M3994-5788,0.,20)
       CALL PICTUR(8.5,4.2,15H CHANNEL NUMBER,
     115,28H SMOOTHED COUNTS PER CHANNEL,28,ACHAN,TBA,216,0.,0)
       END FILE 10
C
       READ 99,BCOUNT,FCOUNT
       IF (BCOUNT)700,700,103
```

```
700 CALL EXIT
    END
```

Acknowledgements

This thesis was made possible through support by the National Science Foundation of the M.I.T. Rockefeller Generator Group, the direction of which was shared by Dr. Leon Beghian and Professor Franklyn Clikeman. The author wishes to express his deep appreciation to Professor Clikeman, who was the supervisor of this thesis.

Thanks go to Mr. James Vaughan for his helpful advice and assistance with the experimental equipment and computer programs; to Mr. Daniel Sullivan who operated the accelerator and contributed his years of valuable experience to the experiment; and to Mr. Anthony Luongo for preparing the lithium target; and Mr. Vernon Rodgers, who also operated the accelerator.

The author is grateful to his wife, Carlene, for typing the thesis; for preparing the diagrams; and last but not least, for her moral support.

The author gratefully acknowledges a Special Fellowship in Nuclear Science and Engineering granted him by the United States Atomic Energy Commission through its contractor, the Oak Ridge Associated Universities.

F.W.G.

Cambridge, Massachusetts

September, 1967